AD NUMBER

AD807412

LIMITATION CHANGES

TO:

Approved for public release; distribution is unlimited.

FROM:

**Distribution authorized to U.S. Gov't. agencies and their contractors;
Administrative/Operational Use; FEB 1967. Other requests shall be referred to Army Electronics Command, Fort Monmouth, NJ.**

AUTHORITY

USAEC ltr 16 Jun 1971

AD

TECHNICAL REPORT ECOM 01698-4

LONG-LIFE COLD CATHODE STUDIES FOR CROSSED-FIELD TUBES

PROGRESS REPORT

by

L. Lesensky - C.R. McGeoch

FEBRUARY 1967

ECOM

UNITED STATES ARMY ELECTRONICS COMMAND · FORT MONMOUTH, N.J.

Contract DA28-043-AMC-01698(E)

RAYTHEON COMPANY
MICROWAVE AND POWER TUBE DIVISION
Waltham, Massachusetts

NOTICES

Disclaimers

The findings in this report are not to be construed as an official Department of the Army position, unless so designated by other authorized documents.

The citation of trade names and names of manufacturers in this report is not to be construed as official Government indorsement or approval of commercial products or services referenced herein.

Disposition

Destroy this report when it is no longer needed. Do not return it to the originator.

Technical Report ECOM-01698-4 February 1967

LONG-LIFE COLD CATHODE STUDIES FOR CROSSED-FIELD TUBES

Fourth Quarterly Report
15 July to 15 October 1966

Report No. 4
Contract No. DA28-043-AMC-01698(E)
DA Project No. 7900-21-223-12-00

Prepared by

L. Lesensky

C. R. McGeoch

RAYTHEON COMPANY
Microwave and Power Tube Division
Waltham, Massachusetts

For

U.S. Army Electronics Command
Fort Monmouth, N.J.

This research is a part of Project DEFENDER, sponsored by the Advanced Research Projects Agency, Department of Defense under Order No. 345, and is conducted under the technical guidance of the U.S. Army Electronics Command, Fort Monmouth, N.J.

ABSTRACT

Secondary emission measurements of electron-beam-evaporated alumina films yielded δ_{max} values of approximately 5.0 with no apparent dependence on film thickness in the range 100 Å - 1000 Å.

Sputtering of 500 Å and 1000 Å electron-beam-evaporated alumina films with nitrogen indicated yields of 0.015 molecules/ion at 0.8 KV and 0.017 molecules/ion at 1.2 KV respectively.

The Hot-Cold Electron Bombardment Vehicle was completed and initial tests performed. Targets requiring activation by high temperature processing will be evaluated.

The 50 kv, S-band Amplitron test vehicle, QKS1194, was nearly completed during present quarter.

Interest and effort on the oxygen approach continues. A high average power version of the QKS1319 CFA test vehicle, which is under construction, will be used for life testing employing the oxygen approach.

An analysis of electron back-bombardment energy, angle of incidence, and phase shift in CFA's is given in the Appendix.

FOREWORD

Long-life cold cathode studies for crossed-field tubes are authorized by the United States Army Electronics Command, Fort Monmouth, New Jersey, under DA Project No. 7900-21-223-12-00. The work was prepared under the support of the Advanced Research Projects Agency under Order No. 345 and is conducted under the technical guidance of the U. S. Army Electronics Command, Fort Monmouth, N. J. 07703.

TABLE OF CONTENTS

LIST OF ILLUSTRATIONS

LIST OF ILLUSTRATIONS (Cont.)

LIST OF TABLES

1. INTRODUCTION

The objective of the present cold cathode study program is to achieve long life cold cathode performance for crossed-field amplifiers. This program is being performed for the United States Army Electronics Command, Fort Monmouth, New Jersey, under contract DA-28-043-AMC-01698 (E).

In this study, selected cold cathode materials will be evaluated as to: their secondary emission properties, their ability to withstand environmental factors expected in a crossed-field amplifier, and their crossed-field amplifier performance. Based on the above experimental information and pertinent theoretical calculations, a life prediction chart will be established for a number of cold cathode materials.

The program is divided into two concurrent phases, phase A being concerned with the measurement of various pertinent properties of cold cathode materials outside of the tube environment, and phase B involving the evaluation and life testing of selected cathodes in a crossed-field amplifier.

The first quarterly report of this contract (Technical Report ECOM 01698-1) contains a discussion of the objectives and plans for the over-all program.

2. PHASE A - MATERIALS EVALUATION

2.1 Electron bombardment vehicle (EBV). During the present report period, EBV activity consisted of the following:

a) Modification of vacuum system and consolidation of power supplies.

b) Measurements on a beryllium (Be) sample.

c) Measurements on a molybdenum alumina ($Mo-Al_2O_3$) film sample.

These are discussed in turn:

2.1.1 EBV system modification. The vacuum system was modified so as to improve its conductance. The 1/2-in. shutoff valve was replaced by a 1-in. bakeable valve which isolates the EBV and Vac-ion pump from the liquid N_2-trapped oil diffusion pump. Significant improvement was thus obtained in the ability to outgas the EBV components.

In addition, the associated power supplies were consolidated in a rack. Figure 1 shows the EBV mounted on top of the table containing the vacuum system. The newly installed 1 in. valve is seen at the right rear of the table. The rack containing the power supplies is located at the right of the vacuum system.

Figure 1. Electron Bombardment Vehicle

2.1.2 Measurements of secondary emission ratio (δ) on a beryllium (Be) sample. A Be sample was mounted in the EBV. The initial value of δ_{max} was 2.25. During the subsequent bombardment for 12.5 hours at 10 amps (corresponding approximately to 1 amp/cm^2) and 1.2 KV, no significant changes in δ occurred. A defective oxygen source was replaced and the system rebaked overnight at 400°C. A leak was discovered and temporarily sealed using anaerobic permafil.

The subsequent measurements of the secondary emission ratio are plotted in Figure 2. δ_{max} is shown as a function of bombardment time at 1 amp/cm^2 and 1.2 KV. The initial high value of $\delta_{max} = 3.43$ decreased in about 2.5 hours to $\delta_{max} = 2.50$, a value which it maintained for approximately 60 hours of bombardment. The initially high δ measurement was presumably due to additional oxidation of the Be target during the overnight bakeout at 400°C with a small leak in the system. As shown in Figure 2, the introduction of O_2 to a pressure of 10^{-5} Torr was not able to restore the higher δ condition.

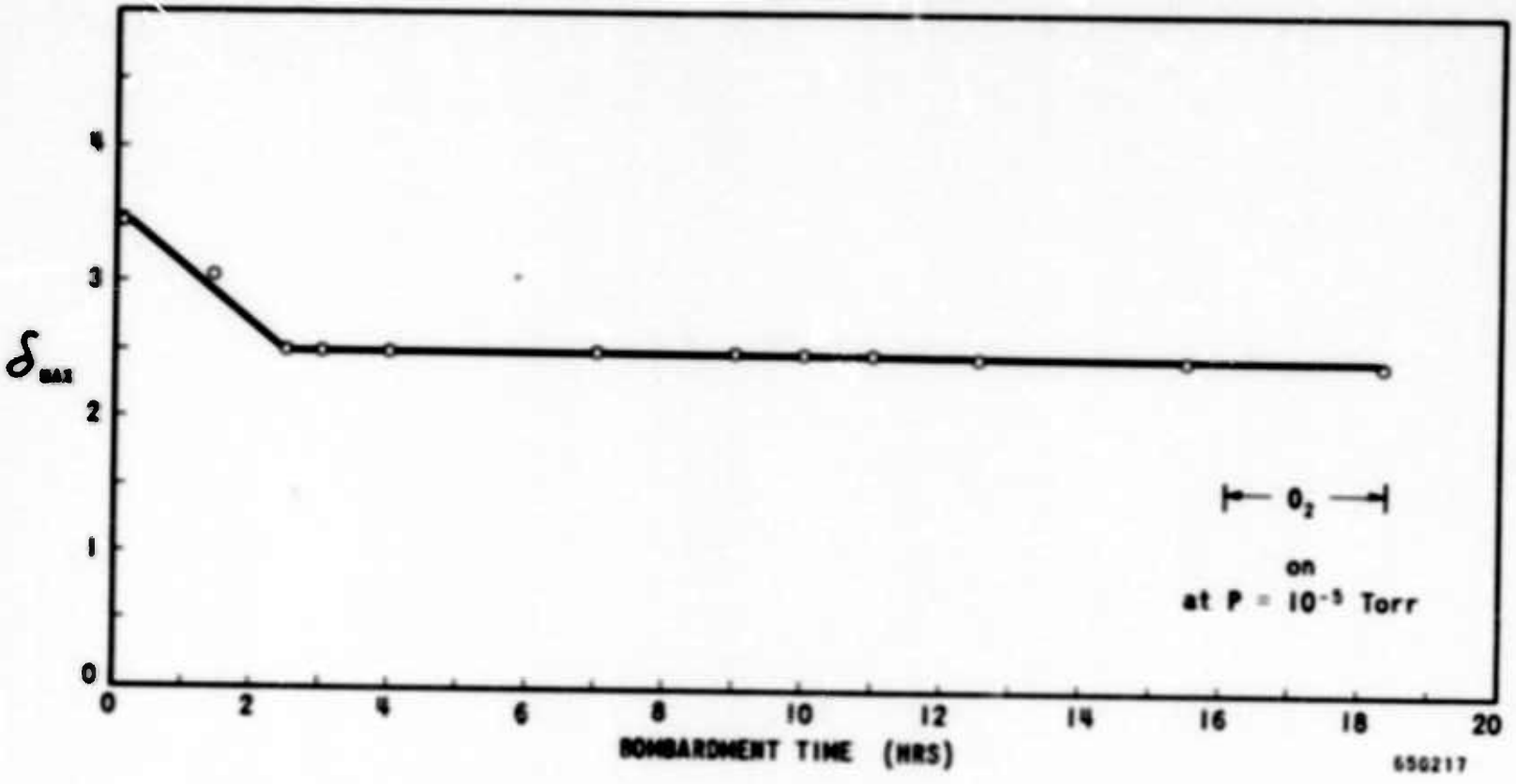

FIGURE 2 Maximum Secondary Emission Ratio vs Bombardment Time at 1 Amp/cm^2 and 1.2 KV for Be Target ($p = 10^{-7}$ torr)

2.1.3 Measurements on a molybdenum alumina (Mo-Al_2O_3) film sample. A 500 Å thick 30% Mo-70% Al_2O_3 film sample on a Mo substrate was mounted in the EBV. Low values of δ_{max} of 1.5 to 1.7 were measured over a 17-hour period of electron bombardment at 1 amp/cm^2 and 1.2 KV. Oxygenation at a pressure of 5×10^{-6} Torr had no apparent effect. Upon disassembly it was noted that some copper had deposited on the target surface, presumably due to an arc to the anode surface near the target.

2.2 Hot-Cold Electron Bombardment Vehicle. The Hot-Cold EBV refers to a version of the EBV completed during the fourth quarter in which the target can be heated by a tungsten radiant heater or cooled by running water through the target base. Figures 3 and 4 show details of the target mount. The tungsten heater mounted in a molybdenum radiation shield, can heat the target to 1100°C, as required for the activation and processing of nickel cermet and impregnated tungsten cathodes. A calibration of this target heater was made in a vacuum bell jar and is shown in Figure 5.

Two barium calcium aluminate impregnated tungsten cathode samples were prepared; one of these was mounted in the Hot-Cold EBV and activated at 1000°C for 30 minutes. δ_{max} was found to be only 1.9. Further activation at 1100°C for 60 minutes resulted in a δ_{max} of 2.2. At this point a short circuit occurred between the anode and target. Upon disassembly of the vehicle, it was noticed that a stainless steel lead had overheated and had deposited metallic evaporants on a ceramic insulator. It is also likely that the target surface had been contaminated. The vehicle is being repaired.

2.3 Ion Bombardment Vehicle. Two electron-beam-evaporated Al_2O_3 films were deposited on a Mo substrate and then sputtered to complete erosion of the film. Due to a slight coloration in the films, it was possible to determine when the film was completely removed; the Mo substrate was then directly visible. The sputtering was performed in N_2 at 10^{-3} Torr and at an ion bombardment current density of 1.2 ma/cm^2 for both films.

The 500 Å film was bombarded at 1.2 KV ion energy and was completely eroded in 15 minutes, corresponding to a sputtering yield of 0.017 mcs/ion. The 1000 Å film was bombarded at 0.8 KV ion energy and was completely eroded in 35 minutes, corresponding to a yield of 0.015 mcs/ion.

For comparison, in the 3rd Quarterly Report of this project, our previous measurement on a 1000 Å 30% Mo-70% Al_2O_3 film implied a yield for Al_2O_3 of approximately 0.007 mcs/ion at an energy of 0.65 KV, while a yield value for Al_2O_3 of 0.016 at 0.65 KV is obtained from Wehner's data.

2.4 Secondary emission measurements. The secondary emission ratios (δ) of several sections of an aluminum cathode which has been run in a non-deteriorated QK1319 CFA were measured. δ_{max} values of 2.06, 2.02, 2.05 and 2.00 were found, while a Pt sample control had a δ_{max} of 1.80. These measurements were made after system bakeout and also an additional heat treatment of the samples at 400°C for 15 minutes. The measured δ's of the aluminum cathode sections were similar to values typically found for untreated aluminum as used in the CFA. We may therefore conclude that CFA operation did not alter the δ of the aluminum cathode.

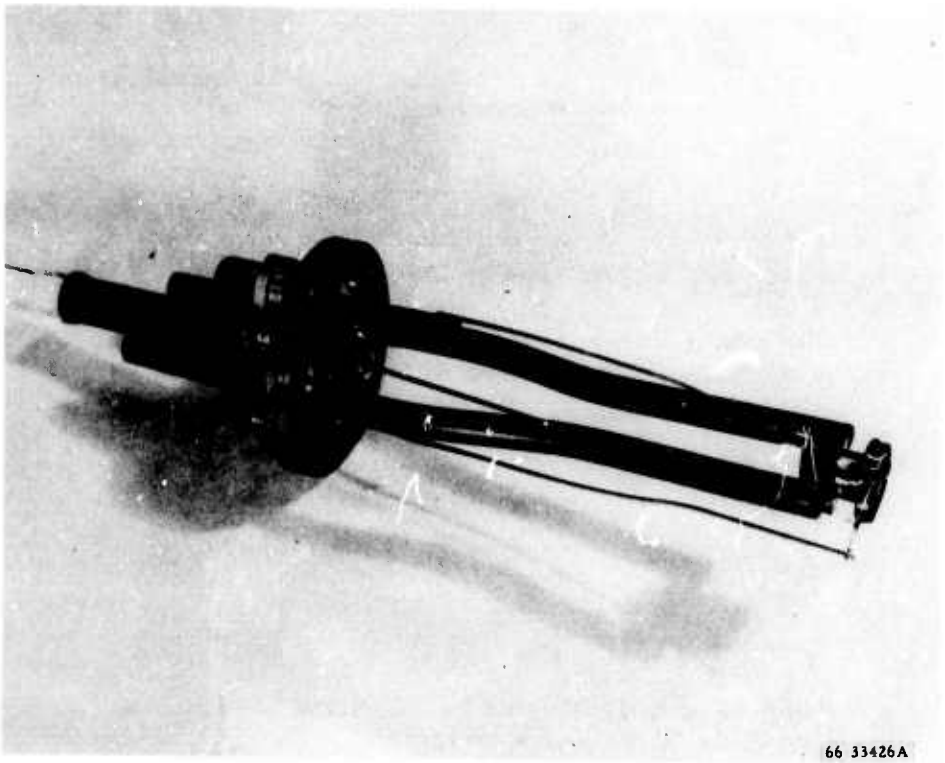

Figure 3. Target Mount and Support Flange
Hot-Cold EBV

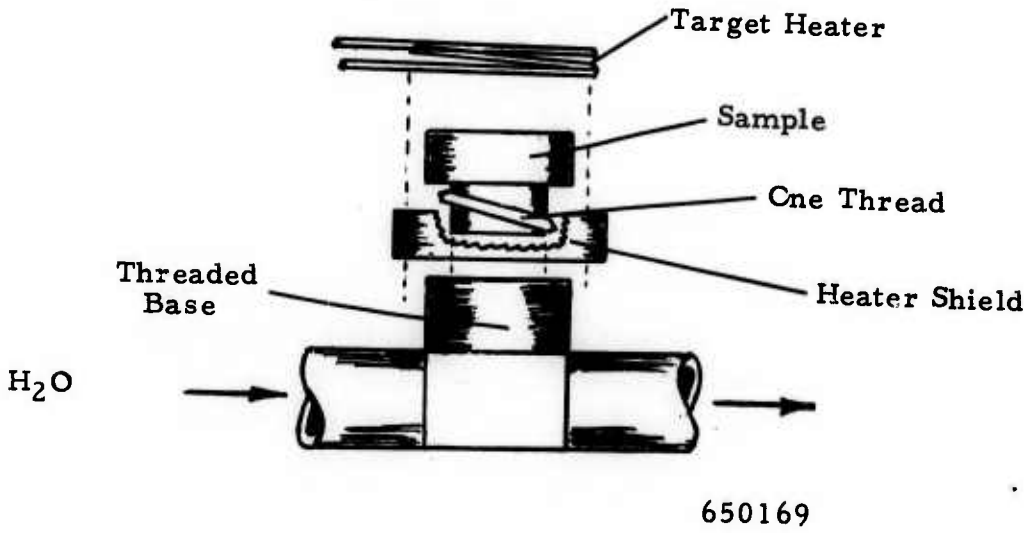

Figure 4. Target Mount of Hot-Cold EBV
(exploded view)

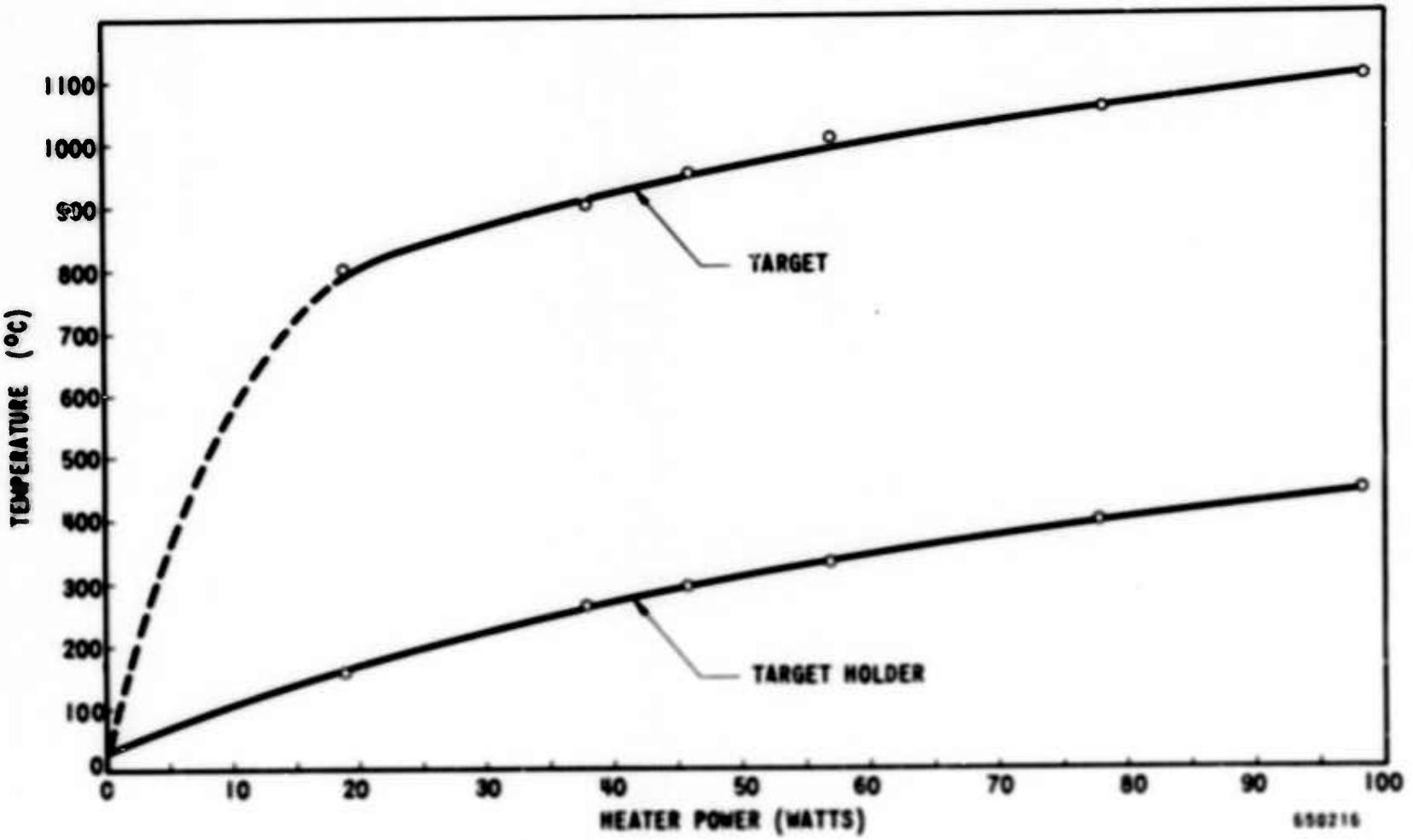

FIGURE 5 Temperature vs Heater Power for Hot-Cold E.B.V.

A series of electron-beam-evaporated Al_2O_3 films were deposited on a Mo substrate and installed in the Secondary Emission Vehicle (SEE). δ_{max} values after outgassing are given in Table I.

Table I.

Film thickness(Å)	Deposition temperature (°C)	δ_{max}	$V_{p\ max}$ (volts)
100	600	4.53	550
100	1100	5.05	475
1000	600	21.0	950
1000	1100	5.52	600

A Pt sample control had a δ_{max} value of 1.88 at 800 volts. The Al_2O_3 films yielded high δ values, in fact somewhat higher than the more typical value of 3.5 to 4 for the 30% Mo-70% Al_2O_3 films described in previous quarterly reports of this program. The δ value of 21 obtained for one of the films is possibly due to a field assisted mechanism, as would occur if tunneling between metallic inclusions was possible. The other three films did not show any charging effects, probably due to the penetration of the primary electrons. A bulk sample of Al_2O_3 (1/16 in. thick) was included in this set and showed charging as expected under dc conditions. The target current remained zero when the voltage of the target support was less than the voltage of the secondary electron collector. This was undoubtedly due to target surface charging to the upper crossover.

3. PHASE B - CFA TESTING

3.1 Hot-Cold CFA test vehicle. Construction is nearly complete of a special QKS1194 Amplitron for use as a test vehicle in evaluating cold cathode emitters which require high temperature activation before operation. The features peculiar to the test vehicle are, for the most part, purely mechanical and do not alter the electrical operating characteristics of the QKS1194 Amplitron which are shown in Table II.

Table II.

QKS1194 Operating Characteristics

Pulse Conditions*	tpc	= 80 μsec
	pps	= 150
	du	= 0.012
Frequency	F	= 2800 - 3200 MHz
Peak drive power	pd	= 50 kw
Peak output power	p_o	≅ 1 Mw
Average output power	P_o	≅ 10 kw
Anode voltage	e_b	≅ 45-55 kv (over operating band)
Peak anode current	i_b	≅ 25 amp
Average anode current	I_b	≅ 275 ma

* May be varied to vary operation characteristics.

A photograph of the QKS1194 is shown in Figure 6. Construction of the anode waveguide assembly has been completed. A change in the design of the welding life will make it possible to evaluate four emitters before any anode re-operation becomes necessary between seal-ins.

A layout of the cathode assembly is shown in Figure 7. By enlarging the inner diameter of the water coolant channel, it is possible to provide space for an immersible heater assembly, which is capable of heating the emitter surface for thermal activation. Possibly, some of the emitters to be evaluated with this vehicle will not require pre-activation; therefore an attempt will be made to start the tube cold, without activation. Caution must be exercised in the event that arcing occurs during this attempt since a severe arc could cause permanent damage to the emitter surface that could not be restored by thermal activation. Once the emitter has been thermally processed, the immersible heater assembly may be removed and coolant tubes inserted for cold cathode operation.

The first emitter to be evaluated will be an impregnated-tungsten-matrix type cathode. Parts for the cathode assembly are complete and construction is in process.

3.2 High average power cold cathode CFA test vehicle. During this report period, the high average power forward wave CFA was sealed-in twice with a beryllium emitter. It was provided with omegatron gauge and Bayard-Alpert gauge appendages for experimental gas analysis during the operation of the O_2 source. The heater-cup assembly of the oxygen source was revised to stabilize the heater power characteristics.

The first experimental hot-test run had to be terminated before cathode deterioration and use of the oxygen source because of a leak which occurred in the glass envelope of the omegatron gauge. The leak was repaired and the test vehicle was again sealed-in and baked out. Unfortunately, an analysis of the gasses evolved during operation could not be performed due to a shorted element in the omegatron gauge.

In both cases, the tube exhibited normal electrical operating characteristics with the beryllium emitter before the termination of the experiment. Experiments will continue to determine the effect of gasses evolved during the use of the oxygen source.

Previous to the use of the Bayard-Alpert gauge appendage, the only provision for recording gas pressure was the Vac-Ion pump itself, making impossible a record of gas pressure without continual operation of the pump. Efforts to "snap on" the Vac-Ion to read pressure without significant pumping action proved to be extremely difficult. Some useful information was obtained when it was observed that cathode deterioration seemed to be reduced by operating without the Vac-Ion pump. However at this time, no definite or conclusive statements may be made on this observation.

A high average power version of the QKS1319 CFA test vehicle containing an oxygen source is currently under construction, under the present program. This tube will be used for life testing purposes. Evaluation of the oxygen approach has also been occurring on another program at Raytheon.

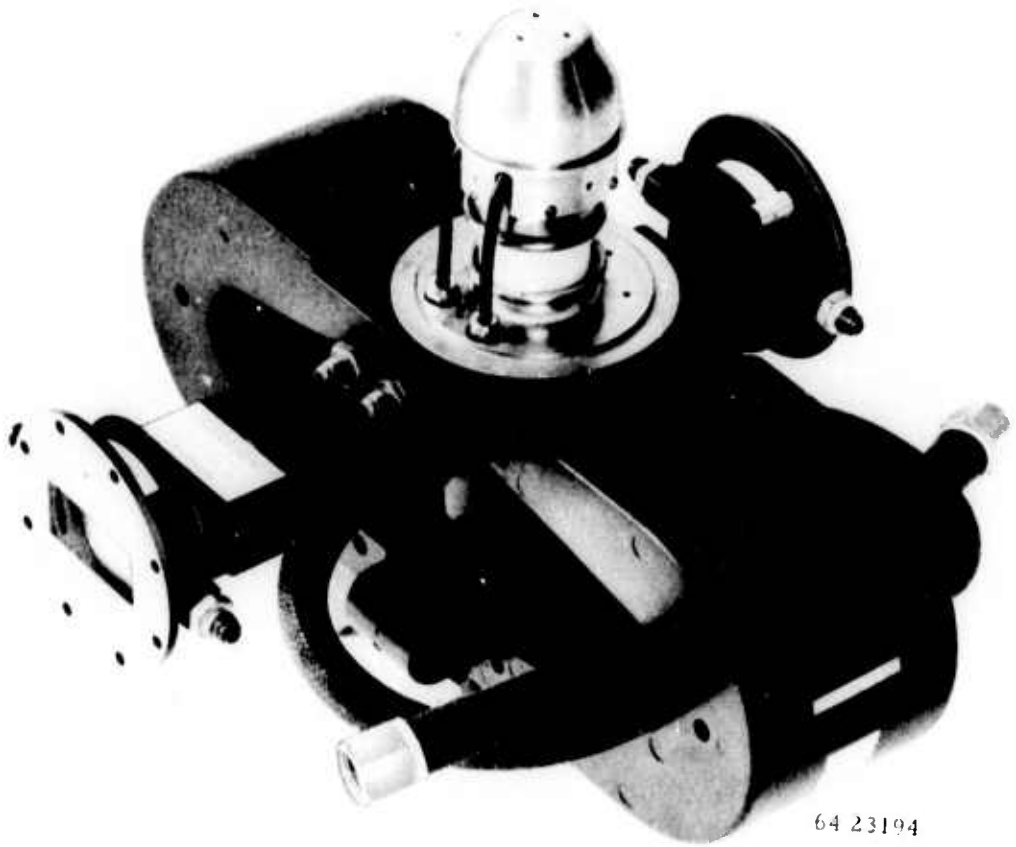

Figure 6. QKS1194 Amplitron

PLANE A-A WATER-COOLED COLD-CATHODE DETAIL

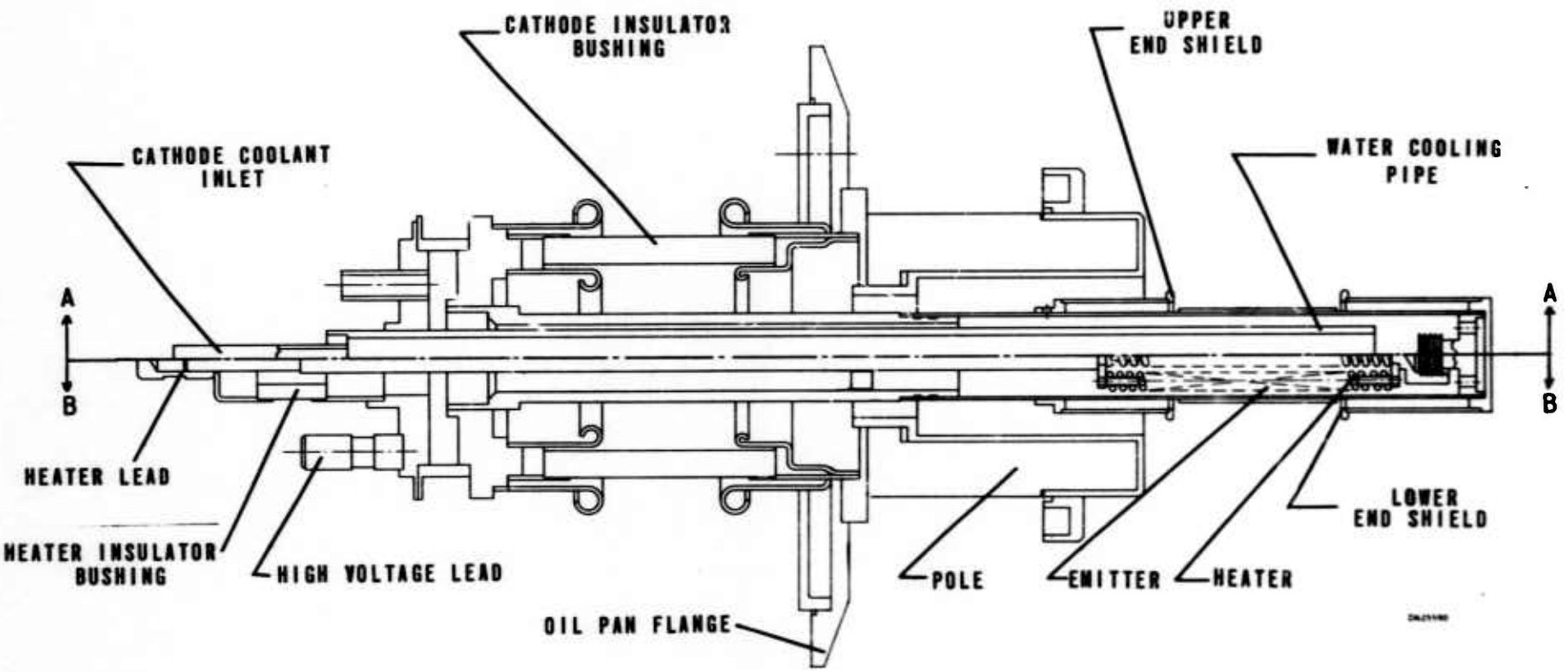

PLANE B-B HOT CATHODE DETAIL

FIGURE 7 QKS1194 Hot/Cold Cathode - Pole Assembly

3.3 Emission current boundaries. The secondary-emission-limited emission current boundary of a CFA employing a cold cathode depends on the effective secondary emission ratio (δ_{eff}) of the cathode surface. The energies and angles of the back-bombarding electrons are unknown.* The effective δ in the CFA therefore can only be estimated.

In the absence of a thermionic contribution, the available anode current may be expressed as

$$I_a = (\delta_{eff} - 1) \quad I_{bb}$$

where

I_a = available anode current

δ_{eff} = effective δ in CFA taking account of energy and angle spectrum of back-bombarding electrons.

I_{bb} = back-bombarding electron current

The dependence of I_a on the anode voltage will depend on the assumption or approximations made for I_{bb}. If we assume that I_{bb} is proportional to I_o, the characteristic current of the crossed-field device, then we obtain the result that I_a is proportional to $V_a^{3/2}$. Thus the perveance represented by the emission current boundary (ECB) would be proportional to $(\delta_{eff}-1)$. However, it is found that a better fit to experimental ECB data of our own and others is obtained by a linear relation of the form

$$I_a = b\,(\delta_{eff}-1)\,(V_a - V_t)$$

V_t is a threshold voltage and reflects the fact that δ decreases to below 1.0 at the "first crossover" voltage. Figure 8 shows emission current boundaries in the QKS1319 CFA test vehicle for several cold cathodes, namely platinum, aluminum, beryllium, and a 1000 Å film of 30% Mo-70% Al_2O_3 on a Mo substrate. If we assume that δ_{eff} for Pt is 1.8, we may compute δ_{eff} for other cathodes in the same CFA by noting that the slope, dIa/dV_a, of the ECB is proportional to $(\delta_{eff}-1)$. The following values of δ_{eff} are thus obtained:

Cold Cathode	δ_{eff}
Al	7.0
Be	5.6
30%Mo-70% Al_2O_3 film	2.2

Secondary emission measurements of an aluminum or beryllium sample, having on its surface a thin oxide film of 25 to 50 Å thick found exposure to 20°C air, yield values of δ_{max} of 2.0 to 2.5. These values much lower than δ_{eff} in a CFA. Optimally oxidized aluminum or beryllium samples, however, do have δ_{max} valves of 4 to 6. Possible explanations of the anomalously high δ_{eff} of aluminum or beryllium cathodes in a CFA are:

1) enhanced back-bombardment current due to presence of thin dielectric film at cathode surface;

* See Appendix

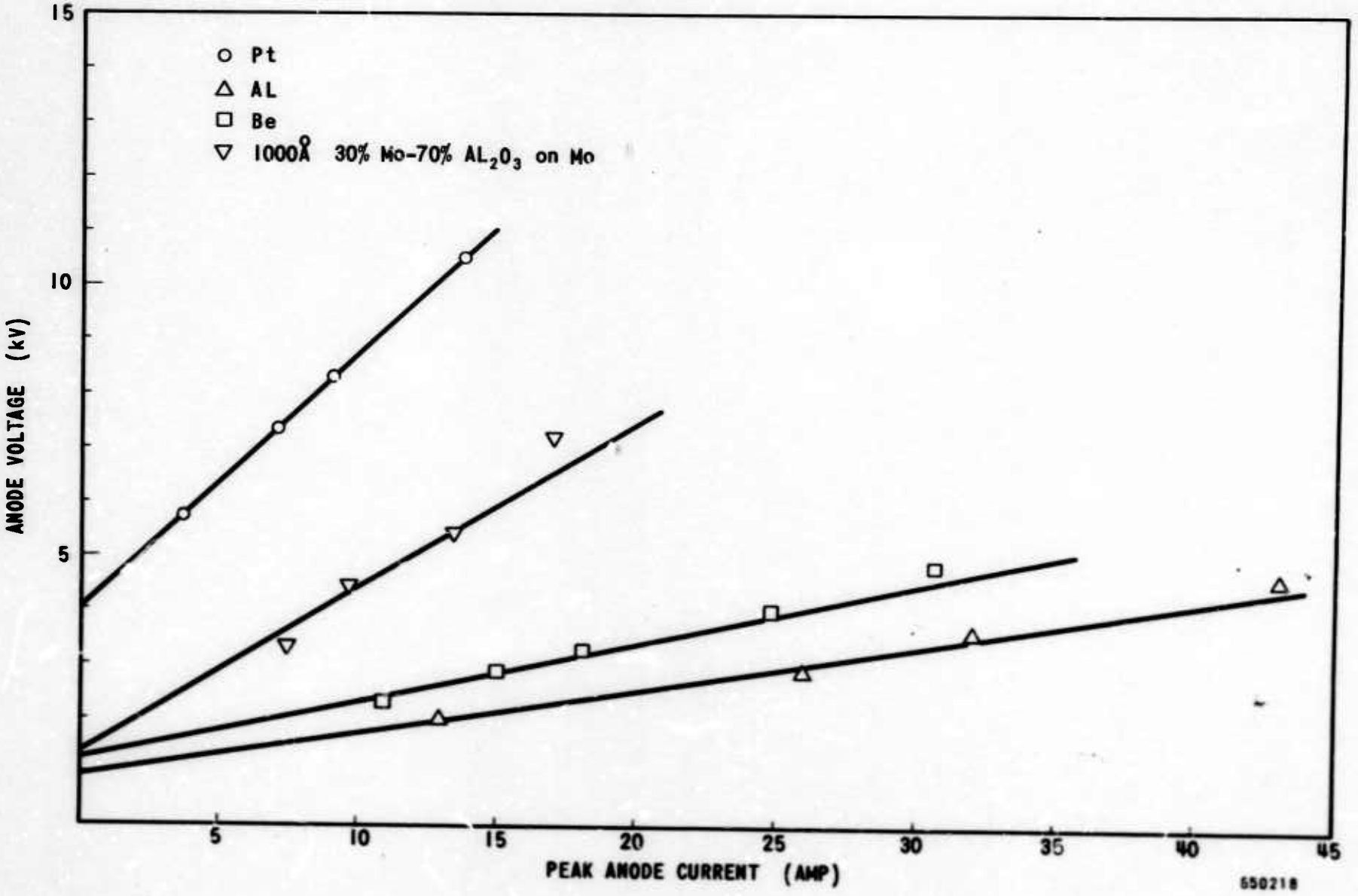

Figure 8. Emission Current Boundaries in QKS1317 CFA Test Vehicles for Various Cathode Materials

2) enhancement of δ due to tube operation, involving a change in nature of oxide film;

3) greater preponderance of grazing incidence for back-bombarding electrons in the case of the oxide film.

3.4 Electron back-bombardment conditions at cathode surface. In order to make the results of the present program applicable to a wide variety of crossed-field amplifiers, more needs to be known about electron back-bombardment parameters and their dependence on dc and rf level.

A brief investigation of this area was therefore initiated by J. M. Osepchuk of Raytheon's Research Division.* The Appendix to the present report describes the results of the study and points out areas of possible further investigation to help elucidate the electron back-bombardment and buildup processes in CFA's.

The electron back-bombardment parameters investigated were energy, angle of incidence, and phase shift. Two cases were investigated:

1) General beam with distribution of orbital amplitudes

2) Cycloidal Beam

The latter case is believed to predominate in the buildup process and in the output region in the steady state and is characterized by near normal incidence, bombardment energy proportional to rf electric field, and short interaction time.

Typically, at saturation power levels, bombardment energy ranges from zero to a maximum of the order of the synchronous beam potential Vo.

Application of this investigation to a study of the buildup process in a CFA is indicated.

* Support for this study was shared by Raytheon Company and the present contract.

APPENDIX A

STUDY OF ELECTRON BACK-BOMBARDMENT ENERGY IN CROSSED-FIELD AMPLIFIERS

by

Dr. J. M. Osepchuk

A-1. INTRODUCTION

The objective of this study is to determine the characteristics of electron back-bombardment in a crossed-field amplifier (CFA) of the distributed emission type – i. e. with a cold cathode yielding a current through the secondary emission process. The characteristics of interest include the distribution of back-bombardment energy, the associated angle of incidence of bombarding electrons, and the resulting shift in phase of secondaries relative to the phase of primary electrons. We wish to know the dependence of these characteristics on interaction space parameters, anode voltage and rf power level. Furthermore, we wish to know how the characteristics differ in several distinct steps of the cold cathode CFA operation, viz.

(1) Buildup stage or initial state
(2) Steady state at rf input
(3) Steady state at saturation locations along interaction length.

In any stage, it is valuable for us to know the location of the secondary emission along the interaction space. Lastly, we are interested in shedding light on possible criteria for buildup and the maximum current boundary, and possible techniques for the enhancement of the process.

The basic geometry of the CFA interaction space is depicted in Figure A-1.

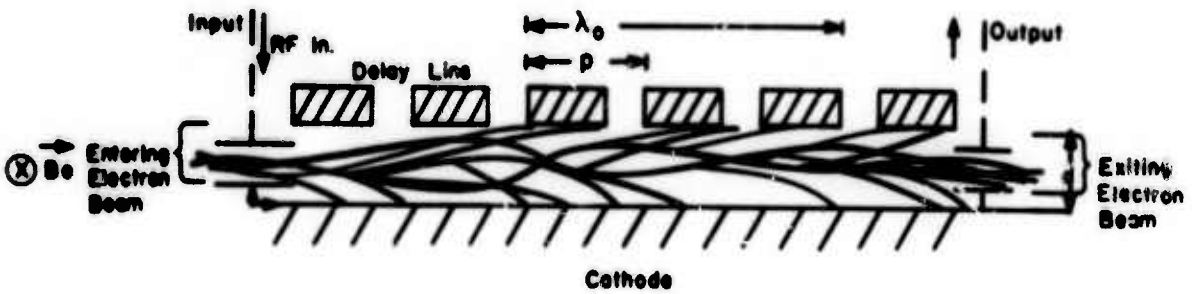

Figure A-1. Interaction Space of Cold Cathode CFA

The device may or may not be re-entrant. If non-reentrant, the electron beam at the input is always zero even in the steady state. If re-entrant, there will generally exist an electron stream entering the interaction space at the rf input which is possibly a modified version of the stream or beam which leaves the interaction space at the rf output. The slow wavelength λ_0 is generally greater than 2 p corresponding to a fundamental phase shift $\psi < \pi$.

The basic process of efficient cold cathode emission is assumed to be the result of interaction under conditions of velocity synchronism, not only for favorable electrons but also for the unfavorable electrons which bombard the cathode. This condition is simply described by the relation

$$(c/v_e) = (\frac{c}{v_o}), \tag{1}$$

where v_o is the phase velocity of the interacting delay line harmonic and v_e is the beam velocity. In this case it is generally assumed that adiabatic conditions exist – which means, in thin beam CFA theory, that $\omega_c/\omega D > 5$ where ω_c is the radian cyclotron frequency. In crude terms this means that any spiralling or relative motion of electrons as caused by the rf fields is small in orbital diameter compared to the cathode-to-anode spacing, so that, in general, the electrons move under the influence of rf fields with a slow drift at a velocity given by (E rf/B). It is the "slow" drift of electrons in unfavorable phase toward the cathode which then leads to back-bombardment and secondary emission at the sole.

This interaction is thus the desired and principally observed effect in CFA cold cathode emission, but note should be taken of various other "spurious" effects which could affect the back-bombardment process if present. These effects are generally associated with cyclotron waves or modes which occur when

$$\frac{c}{v_o} = \frac{c}{v_e} \left(1 \pm \frac{\lambda}{\lambda_c}\right) = \frac{C}{v_e} \left(1 \pm \frac{\omega_c}{\omega}\right), \tag{2}$$

where v_o is the phase velocity of any interacting wave or harmonic, v_e is the beam velocity or the average translational velocity of any part of a beam or stream if there is velocity slip due to space charge, λ is the free space wavelength, and λ_c is the free-space wavelength at the cyclotron frequency. If $\omega_c << \omega$ there is significant cyclotron wave interaction with the fundamental interacting spatial harmonic, but this case is presumed not pertinent since this corresponds to low magnetic fields and non-adiabatic electron motion, both of which are not characteristic of practical CFA's. If $\omega \sim \omega_c$, which is roughly the situation for most CFA's, then, without velocity slip in the beam, there is very little cyclotron-wave interaction except if a "zero mode" or high velocity spatial harmonic exists. In addition, if velocity slip exists there could be significant interaction with slow electrons and the fundamental harmonic. If $\omega_c >> \omega$, there will be no cyclotron interaction with the delay line fields at the operating frequency.

In general, there could be a cyclotron mode interaction at any ω and ω_c if there exist spatial harmonics which satisfy one of the resonance relations of Equation 2. If these spatial harmonics have a significant transverse rf electric field at the cathode, there would result a significant change in the bombardment energy.

The principal extraneous cyclotron mode effects occur because of the existence of "zero mode" or fast wave rf fields which generally can exist in the interaction space because of the insulation between cathode and anode. The delay line may or may not be coupled to such fast TEM waves but their presence can affect back-bombardment, especially if there exist resonances of the fast waves. If the fast waves are coupled to the delay line, they influence the back-bombardment in proportion to the main rf power level on the delay line. Even if uncoupled, these fast waves can influence cathode back-bombardment through independent modes of oscillation.

Although these effects can be important in practice, they are neglected here and omitted from detailed consideration. Nevertheless, their existence and potential importance are recognized.

The present study is made with principal reference to forward-wave interaction in CFA's, although some of the results are of possible application to backward-wave interaction. The latter is potentially a more complicated situation because of possible feedback effects involving the emission process and also because the beam motion is more likely to be nonadiabatic, because of the large rf field level at the beam input and the rapid decrease of rf power level in the beam direction in some cases.

In order to study the perturbed electron motion under the influence of the rf fields, one must first assume a model of the dc beam or electron motion in the absence of rf fields. It is reasonable to assume a distribution of space-charge free electron trajectories for the following reasons: first, in the initial state, or during rf buildup, there is little emission and beam current. Secondly, in the steady state along the locations of high rf power level, it is likely that the beam is far from fully saturated and most of the beam originating in this region results from secondary emission following near cycloidal trajectories of the "primary" electrons in any stage of the multiplication process of secondary emission. Lastly, in the steady state and near the rf input, even if it is conceivable that a near-Brillouin or laminar-flow beam exists, it should be quite rapidly completely distorted into a nonlaminar flow resembling a double stream or multiple stream beam. This, in turn, qualitatively resembles the space-charge free beam (or beam of no velocity slip) rather than an ideal laminar Brillouin beam of full velocity slip. Some study of a perturbed Brillouin beam is possible even within the context of an adiabatic theory. However, the detailed considerations lead to internal contradictions in that, in order to preserve some resemblance of laminarity, the rf fields must be exceedingly small and can lead to no significant electron bombardment per se. It is true, however, that the laminar Brillouin beam theoretically is unstable even without delay line rf fields and should quickly degenerate into a large signal "diocotron" state in which large cathode back-bombardment exists.

These space-charge effects are well known and lead to cold emission in magnetron diodes.[1] In this case, it is found that, without a delay line, cold cathode emission occurs most easily if the space charge wavelength $\lambda_e = d$, the cathode-to-anode separation, and if the cycloidal trajectory period matches the space charge bunch separation, $\lambda_c' = \lambda_e$,

(where $\lambda_c' = \frac{\lambda_c}{(\frac{c}{v_e})}$ and λ_c is the free-space wavelength at the cyclotron frequency), i.e.

$$f_c = f_d = \frac{v_e}{\lambda_e} \cong \frac{V_a}{dB_o \lambda_e} = \frac{V_a}{d^2 B_o} , \qquad (3)$$

or, since $f_c = \frac{1}{2\pi} \eta B_o$,

$$\chi = \frac{V_a}{\frac{\eta d^2 \beta_o^2}{2}} = \frac{V_a}{V_{ac}} = \frac{1}{\pi} . \qquad (4)$$

These space-charge effects are very important and are sure to enter into the consideration of cold cathode effects in a CFA at some point, but they will not be studied here. It is assumed that they are not the principal cause of back-bombardment, but rather that the imposed rf drive is the principal cause.

It is interesting to note, however, that the work with cold cathode magnetrons [Equation (1)] implies that, with a circuit present, the easiest bunching and cold cathode operation results if the circuit slow wavelength λ_o is equal to 2d, and if the cycloid period is half the slow wavelength, i.e.

$$f_c = 2f_d = \frac{2 V_a}{2d^2 \beta_o} = \frac{2v_o}{\lambda_o} = 2f , \qquad (5)$$

where v_o is the phase velocity of the interacting harmonic, or

$$\chi = \frac{V_a}{V_{ac}} = \frac{1}{\pi} , \qquad (6)$$

which is the same condition as before. This implies that

$$\Gamma_o d = \frac{2\pi d}{\lambda_o} = \pi , \qquad (7)$$

which is a somewhat different condition than is generally assumed to be optimum in CFA interaction without distributed emission – namely $\Gamma_o d \sim 2$. The condition given by Equation (5) implies that $\omega_c/\omega = 2$ and that the cycloidal length is equal to one-half the slow wavelength. The condition given by Equation (7) may be optimum for large space-charge effects, but it is assumed that the condition $\Gamma_o d \sim 2$ may be more important for a circuit-driven CFA.

The dc beam model is thus assumed to consist of space-charge free trajectories. In the case of the initial buildup and the entering beam in the steady state, it is likely that a distribution of trajectories from

rectilinear to epicycloidal or trochoidal exist because of the influence of end shields and other perturbations in altering trajectories. The most likely trajectory is assumed to be near-cycloidal because of the origin of all electrons at the cathode. Each trajectory exhibits the same drift velocity $v_e = V_a/a_o$ and an orbital diameter 2R so that the trajectory position is described by

$$\text{average position} \qquad \frac{x_o}{d} = \frac{(1+\rho^2)}{4}\,\chi \tag{8}$$

$$\text{minimum position} \qquad \frac{x_i}{d} = \left(\frac{1-\rho}{2}\right)^2 \chi \tag{9}$$

$$\text{maximum position} \qquad \frac{x_2}{d} = \left(\frac{1+\rho}{2}\right)^2 \chi \tag{10}$$

where $\rho = R/R_o$ and R_o is the radius of a cycloidal orbit, viz

$$R_o = \sqrt{\frac{2\eta V_o}{\omega_c}}\ , \tag{11}$$

the beam potential V_o being

$$V_o = \frac{1}{2\eta}(v_e)^2 = \frac{1}{2\eta}\,\frac{V_a^2}{d^2\beta_o^2} = \frac{1}{4}\chi \cdot V_a\ .$$

In a typical state during buildup or at the entrance in the steady state, it is assumed that the beam is composed of a set of trajectories, uniformly distributed along y and z, and with a weighted probability of ρ, is given by

$$\omega(\rho) = \sin \rho\frac{\pi}{2} \quad ; \quad 0 < \rho < 2\ . \tag{13}$$

For the nature of the "beam" or bombarding primaries along the output section of a CFA in a steady state, it is assumed that all electrons are initially cycloidal trajectories as would result with secondary electrons emitted in a space-charge free region.

Although this picture of the initial dc states neglects dc and ac space-charge effects it showed a valid qualitative and then quantitative picture of the dependence of electron back-bombardment on rf power level and interaction space parameters. The presence of space-charge effects can then be examined for additional effects such as those which influence the buildup or maximum current boundary.

So far, solution for electron trajectories has been obtained for two cases, (1) a general beam with a distribution of orbital amplitudes, and (2) the cycloidal beam. Qualitatively, the first case is characterized by long drift times, finite and considerable back-bombardment energy at low power, and near grazing angles of incidence. The cycloidal trajectory

tends to predominate, however, and weights the results away from these orbital values toward those characteristic of cycloidal bombardment. This latter case is characterized by near normal incidence, bombardment energy proportional to rf electric field, and short interaction time.

The cycloidal case was studied in more detail, with particular examination of phase shift characteristics because of their significance in the sequence of cycloids which make up a multiplication process.

Typically, at saturation power levels, bombardment energy ranges from zero to a maximum of the order of synchronous beam potential, V_o. At power levels 20 dB down from saturation, the bombardment energy is typically a maximum of about 0.2 V_o in the cycloidal case and ranges from (0.17 - 0.34) V_o in the general beam of adiabatic properties.

It is likely that the results of the cycloidal case are of significance to the buildup and output region of the steady state. The results for the more general beam are probably of significance to the input region but only in cases of a re-entrant beam which passes through a significant drift region.

In the next section, theoretical expressions for cathode back-bombardment parameters are derived on the basis of adiabatic theory.

The theory predicts optimum conditions for back-bombardment which are close to those usually assumed for optimum crossed-field interaction with circuit waves. These conditions differ from those stated in the literature for optimum space-charge interaction in the presence of a circuit. For circuit-driven interaction, it is concluded that the space-charge interaction is of secondary importance in most cases.

In the last sections of the report, the results of this study are compared with similar studies of the magnetron, a typical numerical case, and are considered compatible if one takes into account the peculiar effects which result from assuming a Brillouin hub in the magnetron even in the presence of rf interaction.

Application of these results to a study of the buildup process could be made if pertinent data on the secondary emission ratio as a function of primary energy and angle of incidence is made available for cathode materials of interest.

A-2. ADIABATIC THEORY OF CATHODE BACK-BOMBARDMENT

A-2.1 General adiabatic solution. The efficient operation of crossed-field devices has always been associated with adiabatic electron motion as first described for the magnetron, in which electrons drift along rf equipotentials at velocities E_{rf}/β so small and with so little rf-induced orbital energy that the kinetic energy of electrons upon collection at the anode or cathode is essentially derivable from the initial dc trajectory. In this case, the rf fields merely effect the displacement of electrons in the $\pm x$ directions such as necessary for conversion of potential energy and, at the same time, effecting the $\pm y$ displacement pertaining to the phase-focusing process which results in bunches or spokes.

It is assumed that the beam composed of electrons of a distribution of orbital amplitudes, as described in the preceding section, moves at a velocity v_e in synchronism with a fundamental spatial harmonic of phase velocity v_o. We will consider an arbitrary part of the beam of orbital amplitude $a = \rho R_o$ uniformly distributed at the average beam position x_o as depicted in Figure A-2. The initial phase of the electrons in the moving reference frame of the rf field is given by $\phi \simeq \gamma_o y - \omega t$, where $\phi = 0$ is defined as the favorable phase as depicted in Figure A-2. Shown are the rf electric field lines for the fundamental spatial harmonic. The electrons in the range $-\pi/2 < \phi < \pi/2$ are favorable electrons which drift immediately to form a favorable bunch around $\phi = 0$ and drift to the anode. The electrons in the range $\pi/2 < \phi < 3\pi/2$ are unfavorable in the sense that they all initially drift to the cathode in the consequent absorption of rf energy, although electrons near $\phi = \pi/2, 3\pi/2$ (near points B, D) soon cross over to the favorable region and drift to the anode.

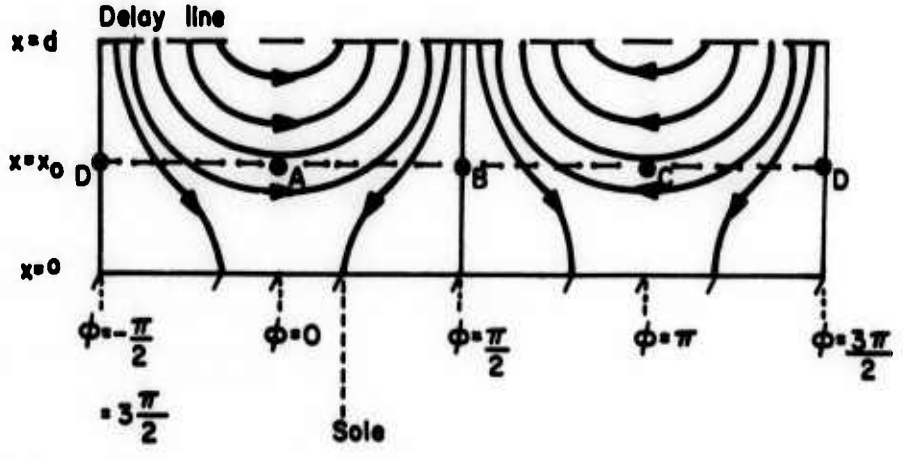

Figure A-2. Electron Beam in Moving Reference Frame of Fundamental Spatial Harmonic

The assumed rf electric field in this moving reference frame is given in its x and y components, assuming no variation in the z direction.

$$E_{1x} = \frac{E_{10} \cosh \gamma_o x \sin \gamma_o y}{\sinh \gamma_o d} \tag{14}$$

and

$$E_{1y} = \frac{E_{10} \sinh \gamma_o x \cos \gamma_o y}{\sinh \gamma_o d} \tag{15}$$

where E_{10} is the amplitude of E_{1y} at the delay line surface and is related to the power flow P by the coupling impedance $R_c(d)$ evaluated at the delay-line surface, viz.,

$$E_{1y} = \gamma_o \sqrt{2R_c(d)\,P} \,. \tag{16}$$

According to the adiabatic assumption, electrons drift along rf equipotentials with a velocity $v = \sqrt{v_{1x}^2 + v_{1y}^2}$ where $v_{1x} = E_{1x}/B^\circ$; and $v_{1y} = E_{1y}/B^\circ$. The rf potential U is given by

$$U = -\frac{E_{10}}{\gamma_o \sinh \gamma_o d} \sinh \gamma_o x \sin \gamma_o y \,. \tag{17}$$

Therefore, the mean trajectory of any electron originating at $x = x_o$, $\phi = \gamma_o y_o = \phi_o$ is described by

$$\sinh \gamma_o x \sin \phi = -\frac{\gamma_o U_o \sinh \gamma_o d}{E_{10}} = \sinh \gamma_o x_o \sin \phi_o \,. \tag{18}$$

The drift velocity v_{1x} is given by

$$v_{1x} = \frac{E_{1y}}{B_o} = \frac{dx}{dt} = \pm \frac{\sqrt{\sinh^2 \gamma_o x - \sin^2 \phi_o \sinh^2 \gamma_o x_o}}{B_o \sinh \gamma_o d} \cdot E_{10} \tag{19}$$

where the ± sign indicates motion toward the anode or the cathode for the two cases respectively of $-\pi/2 < \phi_o < \pi/2$; and $\pi/2 < \phi_o < 3\pi/2$. This equation can be rewritten in a form suitable for direct integration, viz,

$$\frac{\pm \gamma_o \, dx}{\sqrt{\sinh^2 \gamma_o x - \sin^2 \phi_o \sinh^2 \gamma_o x_o}} = \frac{f(t)\,dt}{\tau} \tag{20}$$

where τ is a time constant defined by

$$\tau = \frac{B_o \sinh \gamma_o d}{E_{10}(0) \cdot \gamma_o} \,, \tag{21}$$

$E_{10}(o)$ is the field amplitude at time t = 0 or y = 0 at the beginning of the interaction space, and f(t) describes a possible time variation of the field as seen by moving electrons, i.e.,

$$E_{10} = E_{10}(o)\, f(t) \,. \tag{22}$$

The time constant τ can be interpreted as the time an electron under the influence of the peak electric field $E_{10}(o)$ takes to drift the distance $(\sinh \gamma_o d)/\gamma_o$, which is equal to d for small γ_o and for most practical cases is of the order of (1-3) · d. It is clear, therefore, that actual electron lifetimes should be generally greater than τ, the more so as x_o/d approaches zero.

Equation (20) is directly integrable, using the substitution $u = \sinh^2 \gamma_o x - \sin^2 \phi_o \sinh^2 \gamma_o x_o$ and Pierce's tables (No. 113). The general results are given for the electron position at time T,

for $-\frac{\pi}{2} < \phi_o < \frac{\pi}{2}$

$$\sinh \gamma_o x = \frac{\{\sin^2 \phi_o + [1 + \cos \phi_o]^2 e^{\frac{2g(T)}{\tau}}\} \sinh \gamma_o x_o}{2e^{\frac{g(T)}{\tau}} \cdot [1 + \cos \phi_o]} \tag{23}$$

where $g(T) = \int_0^T f(t)\, dt$, and

for $\frac{\pi}{2} < \phi_o < \frac{3\pi}{2}$

$$T < T_m \quad \sinh \gamma_o x = \frac{\{[1 + |\cos \phi_o|]^2 + e^{\frac{2g(T)}{\tau}} \sin^2 \phi_o\} \sinh \gamma_o x_o}{2e^{\frac{g(T)}{\tau}} [1 + |\cos \phi_o|]} \tag{24}$$

$$T > T_m \quad \sinh \gamma_o x = \frac{\left(1 + e^{\frac{2g(T, T_m)}{\tau}}\right) |\sin \phi_o| \sinh \gamma_o x_o}{2e^{g(T, T_m)}} \tag{25}$$

where

$$\frac{T_m}{\tau} = \ln \left[\frac{1 + |\cos \phi_o|}{|\sin \phi_o|}\right] \tag{26}$$

and

$$\frac{g(T, T_m)}{\tau} = \int_{T_m}^{T} f(t)\, dt\,. \tag{27}$$

The time T_m defines the time any electron in the unfavorable phase region ($\pi/2 < \phi < 3\pi/2$) takes to drift to phase $\phi = \pi/2$ or $3\pi/2$ after which it drifts upward to the anode. This shows that all electrons except the one exactly at $\phi_o = \pi$ eventually drift to the anode and are not intercepted by the cathode if their orbital amplitude $a = \rho R_o$ is zero. If an electron has a finite orbital amplitude a, then it is found that only those electrons with ϕ_o in the range of $\pi - \phi_m < \phi_o < \pi + \phi_m$ are intercepted by the cathode where

$$\sin \phi_m = \frac{\sinh \gamma_o a}{\sinh \gamma_o x_o} \tag{28}$$

and the time of interception is given by Equation (24) with $x = a$. This time is approximate within one cyclotron period – i.e., the actual time of interception could be anywhere between the time given by Equation (24) for $x = a$, and a time longer by one cyclotron period. In most practical cases where the adiabatic theory is of value this is a small difference.

Another interpretation of Equation (28) is that the minimum position x_m for a trajectory beginning at ϕ_o, x_o is given by

$$\sinh \gamma_o x_m = \sin \phi_o \sinh \gamma_o x_o \tag{29}$$

where $\phi = \pi/2$, or $3\pi/2$ when $x = x_m$.

Given x(T) one can in general determine y or $\phi = \gamma_o y$ from (18), i.e.,

$$\sin \phi = \frac{\sinh \gamma_o x_o \sin \phi_o}{\sinh \gamma_o x} \quad . \tag{30}$$

The results for x(T) can be rewritten in a form more suitable to determining T(x), viz,

$$-\pi/2 < \phi < \pi/2$$

$$\frac{g(T)}{\tau} = \ln \left[\frac{\sinh \gamma_o x \left(1 + \sqrt{1 - \dfrac{\sin^2 \phi_o \sinh^2 \gamma_o x_o}{\sinh^2 \gamma_o x}}\right)}{\sinh \gamma_o x_o \left(1 + \cos \phi_o\right)} \right] \tag{31}$$

$\pi/2 < \phi < 3\pi/2$

$$T < T_m(\phi_o) \qquad \frac{g(T)}{\tau} = \ln \left[\frac{\sinh \gamma_o x_o \, (1 + |\cos \phi_o|)}{\sinh \gamma_o x \left(1 + \sqrt{1 - \sin^2 \phi_o \, \frac{\sinh^2 \gamma_o x_o}{\sinh^2 \gamma_o x}}\right)} \right] \tag{32}$$

$$T > T_m(\phi_o) \qquad \frac{g(T, T_m)}{\tau} = \ln \left[\frac{\sinh \gamma_o x \left(1 + \sqrt{\frac{1 - \sin^2 \phi_o \sinh^2 \gamma_o x_o}{\sinh^2 \gamma_o x}}\right)}{\sinh \gamma_o x_o \sin \phi_o} \right]. \tag{33}$$

If the field E_{10} is not a function of time, i.e., if $f(t) = 1$, $g(T) = T$, $g(T - T_m) = T - T_m$ then expressions (31) - (33) yield explicitly $T(x)$.

Equation (32) can be applied to the problem of interest, namely cathode back-bombardment, to determine the time for a particular electron with orbital amplitude a, and initial coordinates x_o, y_o, to reach the cathode, as follows:

$$\frac{T_a}{\tau} = \ln \left[\frac{1 + |\cos \phi_o|}{\sin \phi_m \left(1 + \sqrt{1 - \frac{\sin^2 \phi_o}{\sin^2 \phi_m}}\right)} \right] \tag{34}$$

An examination of these expressions for τ, T_a, and T_s as a function of $\gamma_o d$, reveals that, for a given beam position and anode voltage (i.e., constant V_a and V_{ac}), and given rf output power, τ/T_c is a minimum when $\tanh \gamma_o d = \gamma_o d/2$ or $\gamma_o d \approx 1.92$. Furthermore, the minimum value of T_a/T_c occurs at $\phi_o = 0$ and, for $\gamma_o d$, a little less than 1.92, if x_o/d is greater than 0.5. If x_o/d is small, then the value of $\gamma_o d$ for minimum T_a will be considerably reduced. In a similar manner, a study of T_s/T_c shows that the minimum value at $\phi_o = \pi$ occurs for a $\gamma_o d$ value a little less than 1.92, if ρ is close to 1, i.e., cycloidal trajectories, but as ρ approaches 0 the value of $\gamma_o d$ for minimum T_s is greatly reduced (T_c = the cyclotron period).

Despite these variations it is clear that values of $\gamma_o d \sim 1.5 - 2.0$ are optimum with respect to the fastest response possible of the beam to a given rf power level under most conditions.

A-2.2 Formulas for cathode back-bombardment under adiabatic conditions. Assuming a beam with space-charge free trajectories and parameters ρ and χ as defined in Section A-1, and using the expressions from adiabatic theory for the superimposed trajectories in the moving reference frame, one can write the following formulas for the properties of cathode back-bombardment under adiabatic conditions. For a given ρ, χ, and $\gamma_o d$, only those electrons with $\pi - \phi_m < \phi_o < \pi + \phi_m$ are collected at the cathode, where ϕ_m is given by

$$\sinh \phi_m = \frac{\sinh \frac{\rho \chi}{2} \cdot \gamma_o d}{\sinh \left(\frac{1+\rho}{4}\right)^2 \chi \cdot \gamma_o d} \cdot \tag{35}$$

The basic time constant τ can be rewritten as

$$\frac{\tau}{T_c} = \frac{\omega_c B_o \sinh \gamma_o d}{2\pi E_{10} \cdot \gamma_o} = \frac{V_{ac}}{\pi(\gamma_o d)^2} \cdot \frac{\sinh \gamma_o d}{\sqrt{2 R_c(d) P_o}} \tag{36}$$

where T_c is the cyclotron period.

The time for collection at the cathode is

$$\left(\frac{T_s}{T_c}\right) = \left(\frac{\tau}{T_c}\right) \cdot \ln \left[\frac{1 + |\cos \phi_o|}{\sin \phi_m \left(1 + \sqrt{1 - \frac{\sin^2 \phi}{\sin^2 \phi_m}}\right)} \right] . \tag{37}$$

The backbombardment energy in volts is bounded by a minimum value given by

$$\left(\frac{V_{bb}}{V_o}\right)_{min} = (1 - \rho)^2 \tag{38}$$

and a maximum value given by

$$\left(\frac{V_{bb}}{V_o}\right)_{max} = (1 - \rho)^2 + \frac{2\rho |\cos \phi_s|}{\frac{\tau}{T_c}} \tag{39}$$

where

$$\sin \phi_s = \frac{\sin \phi_o}{\sin \phi_m} \quad . \tag{40}$$

The minimum value results if the electron is intercepted at the moment of minimum energy or minimum $x = x_1$ in the dc trajectory. The maximum value results if the electron just misses the cathode when $x = x_1$ in the dc trajectory and performs one more orbital trajectory before bombardment. The phase ϕ_s corresponds to the phase of the rf field at the position of collection at the cathode for the particular electron originating at x_o and ϕ_o.

The total phase shift of the electron is

$$\Delta\phi_t = \phi_s - \phi_o + \Delta\phi \tag{41}$$

where $0 < \Delta\phi < \Delta\phi_{max}$ and $\Delta\phi_{max}$ is given by

$$\Delta\phi_{max} = \rho(\gamma_o d)^2 \left\{ \frac{1}{2} \left(\frac{2\pi |\cos \phi_s|}{\sinh \gamma_o d} \right)^{\frac{1}{2}} \frac{V_a}{V_{ac}^{3/2}} (2R_c(d)P_o)^{1/4} - \frac{\pi \cosh\left(\frac{\gamma_o d \cdot V_a}{2V_{ac}}\right) \sin \phi_s \sqrt{2R_c(d)P_o}}{V_{ac} \sinh \gamma_o d} \right\} \tag{42}$$

The angle of incidence of the bombarding electron as defined by deviation from normal bombardment (cf Figure A-3) is given by

$$\Theta_{inc} = \tan^{-1} \left[\frac{1 - \rho \cos \Theta}{\rho \sin \Theta} \right] \tag{43}$$

where $0 < \theta < \theta_{max}$ and θ_{max} is given by

$$\sin \Theta_{max} = \sqrt{\frac{2|\cos \phi_s|}{\tau/T_c} - \left(\frac{\cos \phi_s}{\tau/T_c}\right)^2} \quad . \tag{44}$$

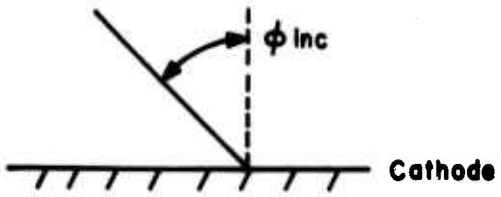

Figure A-3. Definition of Angle of Incidence in Bombardment

If all electrons were collected just at the point of minimum dc kinetic energy, as with weak rf fields and long T_s, then $\Delta\phi$, $\theta = 0$ and

$$\left(\frac{V_{bb}}{V_o}\right) \rightarrow \left(\frac{V_{bb}}{V_o}\right)_{min} .$$

The modifications to the quantities $(V_{bb}/V_o)\,\Delta\phi t$, and θ_{inc} from their limiting values at long T_s are derived from an approximate solution of perturbal cycloidal trajectories described in the next section.

One can see qualitatively that back-bombardment under adiabatic theory implies bombardment energy (38) of the order of V_o or smaller generally $0 < \rho < 2$; little collection for $\rho \sim 0$; maximum collection if $\rho \sim 1$; and angle of incidence close to grazing in general, i.e., $\theta_{inc} \sim \pi/2$.

A-2.3 Cycloidal back-bombardment under conditions of cycloidal trajectories. If the dc trajectories are cycloids, as happens for electrons originating at the cathode by secondary emission, (i.e., $x_1 = 0$, $x_o/d = \chi/2$, $x_2/d = \chi$), then the simple adiabatic theory predicts return to the cathode without back-bombardment energy and an angle of incidence of zero - i.e., normal incidence. Actually, in one cycloidal motion, a significant amount of energy transfer occurs to yield a finite back-bombardment energy and a departure from normal incidence. These quantities are calculated approximately here assuming that the electron in one cyclotron period drifts down a distance Δx given by

$$\Delta x = \frac{E_{1y}}{B} \cdot T_c \qquad (45)$$

where

$$E_{1y} \cong \frac{E_{10} R_o \gamma_o \,|\cos\phi|}{\sinh \gamma_o d} . \qquad (46)$$

Then the energy of bombardment is approximately given by

$$\frac{1}{4}\left(\frac{V_{bb}}{V_o}\right)_{cyc} = \frac{\Delta x}{2R_o} \tag{47}$$

or

$$\frac{V_{bb}}{V_o}_{cyc} = \frac{4\pi}{\omega_c B_o} \frac{E_{10}\gamma_o \cos\phi}{\sinh \gamma_o d} = 2\pi(\chi)\left(\frac{E_{10}}{E_o}\right) \frac{\cos\phi}{\left(\frac{\sinh \gamma_o d}{\gamma_o d}\right)} \tag{48}$$

or

$$\left(\frac{V_{bb}}{V_o}\right)_{cyc} = \frac{2|\cos\phi|}{\tau/T_c} . \tag{49}$$

The angle of incidence is given by

$$\theta_{inc} = \tan^{-1}\left[\frac{1-\cos\theta_c}{\sin\theta_c}\right] . \tag{50}$$

Where θ_c is given by

$$\sin\theta_c = \sqrt{\frac{2|\cos\phi|}{\tau/T_c} - \left(\frac{\cos\phi}{\tau/T_c}\right)^2} \tag{51}$$

which is also the same expression as that (44) for θ_{max}.

The phase shift $(\Delta\phi)_{cyc}$ is influenced by $\overline{E}_{1x}$ as well as $\overline{E}_{1y}$, as it is assumed that $\overline{E}_{1x}$ is approximately given by

$$\overline{E}_{1x} \cong E_{10} \frac{\cosh \gamma_o R}{\sinh \gamma_o d} \sin\phi . \tag{52}$$

Then the phase shift is found to be given by

$$(\Delta\phi)_{cyc} = (\gamma_o d)^2 \left\{ \frac{1}{2} \left(\frac{2\pi |\cos\phi|}{\sinh \gamma_o d} \right)^{\frac{1}{2}} \frac{V_a}{V_{ac}^{3/2}} (2R_c P_o)^{1/4} \right.$$

$$\left. - \frac{\pi (\cosh \frac{\chi}{2} \gamma_o d) \sin\phi \sqrt{2R_c(d) P_o}}{V_{ac} \sinh \gamma_o d} \right\} . \qquad (53)$$

An examination of Equation (49) for the cathode back-bombardment indicates that it is maximum at $\phi = \pi$ and inversely proportional to the basic time constant τ. This means that the bombardment energy is proportional to the square root of the power, inversely proportional to the cutoff voltage V_{ac}, and proportional to $(\gamma_o d)^2/\sinh \gamma_o d$. This latter function is a maximum at the $\gamma_o d$ value for which $\tanh \gamma_o d = \gamma_o d/2$. This value is $\gamma_o d = 1.92$ which is roughly the value of $\gamma_o d = 2$, generally assumed an optimum for effective crossed-field interaction. It is interesting to note, then, that the same value of $\gamma_o d$ is optimum for most effective phase-focusing and also for a given rf power, anode voltage, and average beam position. The value of $\gamma_o d = 1.92$, therefore, also signifies a minimum value of τ/T_c for the same given condition as pointed out earlier.

The incidence is close to normal for low power (i.e., high τ_o), the more so at $\phi \sim \pi/2, 3\pi/2$. For high power levels and especially at $\phi_o = \pi$, the angle of incidence approaches grazing slowly – e.g., $\theta_{inc} = 45^\circ$ at $\phi_o = \pi$, when $\tau/T_c = 1$. The phase shift expression, Equation (53), is composed of two terms, the first related to the effect of E_{1y}, and the second related to the effect of E_{1x}. For $\phi > \pi$, both terms are positive, indicating a shift of the electron in the direction of beam travel. For $\phi < \pi$, the second term is negative and, at some value of $\phi = \phi_e$, the phase shift will be zero. For $\phi > \phi_e$, the phase shift is positive and for $\phi < \phi_e$ the phase shift is negative. The value of ϕ_e is close to $\pi/2$ for low power and shifts toward π at high power. The existence of such a stationary phase point, though unstable, is significant since it implies that such a point in a steady state could be a continuing original source of cold cathode emission as the wave and beam move along in synchronism. This point is discussed later after the numerical results for the example studied in the next section are reviewed.

A-3. NUMERICAL STUDY FOR A TYPICAL CFA

Cathode back-bombardment properties as described by the preceding theory, will be examined for a particular case which may be said to be typical or at least similar to practical CFA's of several types at power levels of 10 kW or more. The basic parameters are assumed to have the following values: $\gamma_o d = 2$, $R_c(d) = 200\Omega$, $V_{ac} = 24$ kV, $V_a = 12$ kV (i.e. $\chi = 0.5$); $\therefore V_o = 1.5$ KV. The choice of $\gamma_o d$ and χ implies a value of $\omega_c/\omega = 2.0$.

It is interesting to note that this example includes the oft-quoted optimum value of 2 for $\gamma_o d$, which is then close to the value for maximum back-bombardment under cycloidal beam conditions, and the value of $\omega_c/\omega = 2.0$ is one of the optimum conditions stated in studies of cold-cathode magnetrons.[1] The value of $\gamma_o d = 2$ is different, however, from the optimum value of π stated in these studies.

The cathode back-bombardment will be evaluated first, discussing a beam of dc trajectories with the distribution $w(\rho) \sin \rho \pi/2$ then, secondly, for cycloidal trajectories originating at the cathode. The results will be examined under the assumption of a constant power level in the range from 0.1 to 100 kW.

In the first case, results are computed for $\rho = 0.1$, 0.5, 0.9, 1.5, and 1.9. These five values are chosen principally to illustrate the variety and the extremes of the behavior of the distribution of trajectories. Therefore, the distributions and averages are not exactly valid but are computed only for a rough illustration of the basic overall properties.

The beam current capacity of this interaction space can be gauged by calculating the pertinent value of the Brillouin laminar beam current which is given by

$$I_o = \frac{2\pi \ell}{\lambda_c} \frac{V_{ac}}{\xi_o} \left[1 - \sqrt{1 - \chi}\right]^2 , \qquad (54)$$

where ℓ is the width of the interaction space, λ_c is the free space wavelength at the cyclotron frequency, and ξ_o is the free space wave impedance $= 372\Omega$. If we assume $\ell/\lambda = 0.25$, then a value of 17.2 A is obtained for the particular CFA example. Thus, if a fully saturated Brillouin beam with this current existed at the input of such a CFA of arbitrary length, a saturated rf power of at least 100 kW is conceivable without additional distributed emission. With sufficient length and sufficient distributed emission, an even larger saturation power level is conceivable if the interaction conditions in the regions of the higher power level are still reasonably adiabatic. If, however, the power level is so high that nonadiabatic motion occurs, then efficiency would begin to fall and such power levels would become academic for such a CFA interaction space. The onset of nonadiabatic conditions can be estimated from an evaluation of the rf potential [cf Equation (17)] as a function of rf power level. For this example the rf potential is equal to $632 \sqrt{P_o}$, where P_o is in kilowatts. Thus, when $P_o = 100$ kW, the rf potential is equal to 6.32 kV, which is comparable with the anode potential of 12 kV. Thus, above 100 kW, decrease of efficiency should result in the additional power transfer because of the onset of nonadiabatic conditions. The onset of nonadiabatic conditions roughly corresponds to $\tau/T_c \sim 1$.

This is exhibited in Figure A-4 which shows τ/T_c-vs-power level from 0.1 to 100 kW for a CFA of the parameters chosen above. This basic time constant depends on the power level as the inverse square root; therefore, over the 1000 to 1 range of power level, the time constant varies from roughly 30 cyclotron periods to about one.

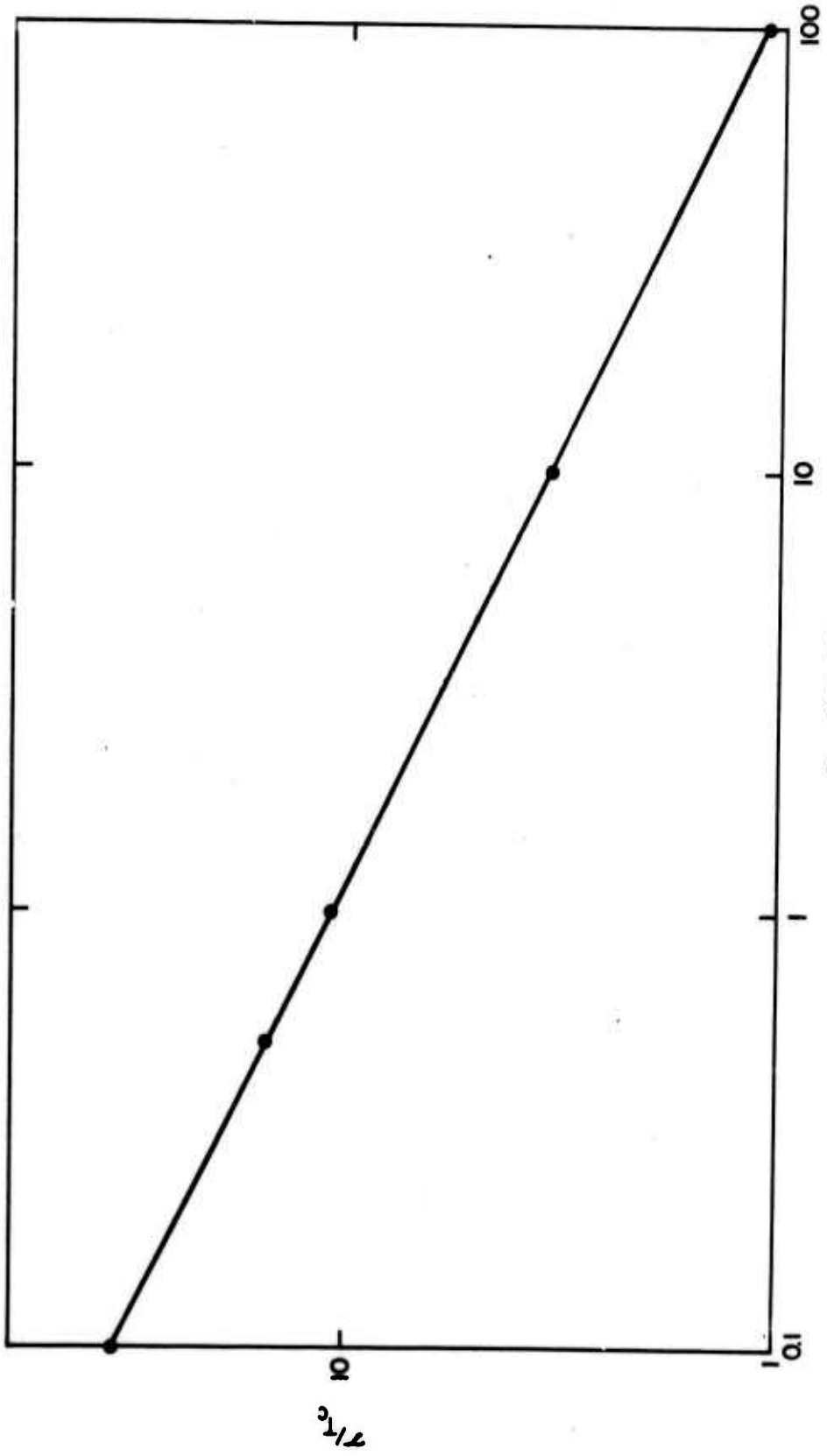

Figure A-4. The Time Constant τ as a Function of Power Level

A-3.1 Adiabatic beam bombardment. The cathode back-bombardment properties in the case of a beam with dc trajectories distributed as $w(\rho) = \sin \rho \pi/2$ will now be reviewed. The results are computed on the basis of adiabatic trajectories and account is made of the deviation from exact adiabatic results because of the finite energy transfer to an electron in the last cyclotron period before impinging on the cathode. The assumed beam is a reasonable guess of the variety of trajectories existing during initial buildup of a cold cathode CFA or in the input region during a steady state. During buildup, initial free electrons may arise from ionization or from secondary emission at the cathode by ion or electron bombardment. In all these cases of origin, the free electrons follow cycloidal trajectories, $\rho = 1$, since they begin their trajectories approximately at rest. Electrons derived from emission at the end shields may follow trajectories with $\rho \neq 1$. In any case, the initial electrons will, in general, possess finite velocity components in the direction of magnetic field. Therefore, after sufficient time, electrons will experience one or several reflections at the end shields which will tend to alter the value of ρ on a random basis either to higher or lower values. In this manner it is reasonable to assume that the distribution of ρ among the electrons, given sufficient time, will be broadened from an initial distribution highly peaked at $\rho = 1$, to a broader distribution such as is assumed. The distribution is still a maximum at $\rho = 1$. Conditions of long drift times before collection can be assumed to exist during buildup or in the case of electrons passing through a drift region between the output and input of a re-entrant CFA. In the latter case, it is assumed that the space-charge density is much smaller than the Brillouin value so that space-charge forces only alter the values of the orbital parameters of the trajectories by a small-to-moderate degree from space-charge free values but do not completely suppress the orbital nature of beam trajectories, which would have to be recognized if the space-charge density were the full Brillouin value.

The time T_s for electrons in appropriate phases to drift to the cathode under adiabatic conditions is plotted in Figure A-5 for five values of ρ. This time is proportional to the basic time constant τ which depends on power level, but otherwise the relative variation of T_s with initial phase ϕ_o and orbital amplitude ρ is independent of power level. Several important features of the adiabatic electron motion are demonstrated on this figure. For a given ρ, only those electrons with initial phase ϕ_o in the range of $\pi - \phi_m < \phi_o < \pi + \phi_m$ are collected by the cathode, where ϕ_m is given by Equation (35). The total range $2\phi_m$ is zero at $\rho = 0$ and approaches zero at large ρ. This means that a beam of rectilinear trajectories within the assumptions of adiabatic motion is not collected at the cathode at all. Since rectilinear trajectories in a laminar beam is the assumption of most non-linear theories of crossed-field devices, it is not surprising to observe that these theories provide no information on cathode or sole bombardment. The fact that ϕ_m approaches zero at large ρ indicates that electrons of large ρ are of little significance for cathode bombardment. The range ϕ_m has a maximum at $\rho = 1$, the cycloidal trajectories with a minimum $T_s = 0$, i.e. neglecting a one cycloid period in the electron lifetime. The actual drift times are as large as 20 or more cyclotron periods for $P_o = 1$ kw or lower and $\rho = 0.1$. For orbital amplitudes close to unity, e.g., $\rho = 0.9$, the actual drift times are quite small, in general less than one cyclotron period even at power levels of 0.1 kilowatt.

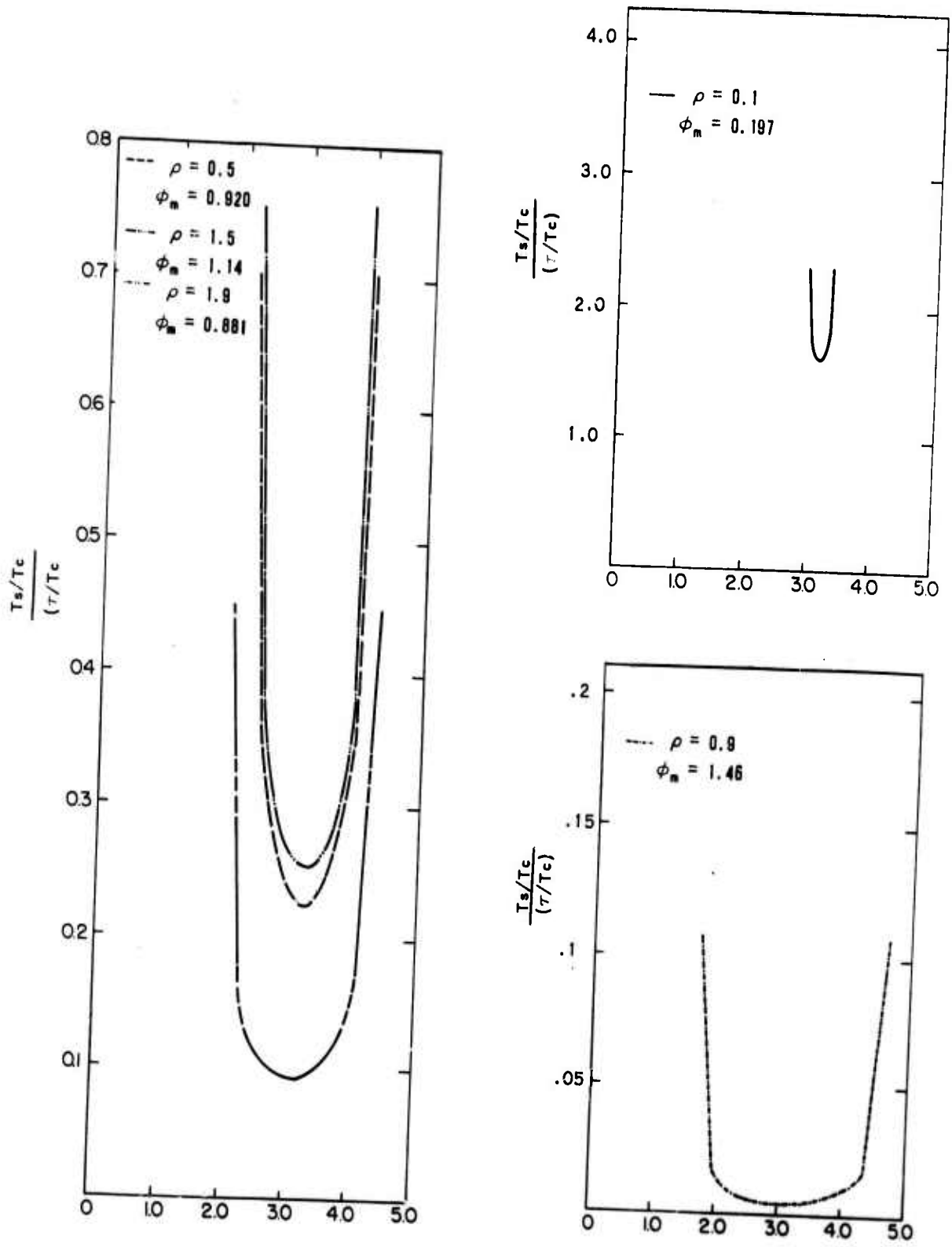

Figure A-5. Electron Drift Time to Sole Under Adiabatic Motion vs Phase for Several Orbital Amplitudes

From this one aspect of adiabatic beam bombardment of the cathode, one can see several reasons why the cycloidal trajectory and its characteristics should predominate. First, it was assumed in the distribution $w(\rho) = \sin \rho\, \pi/2$, that the cycloid or near-cycloid trajectories are most probable. Second, assuming that trajectories of any ρ are distributed uniformly in initial phase, it is only for $\rho = 1$ that 50% of the trajectories intercept the cathode. For $\rho = 0.1$, for example, only six% of the trajectories intercept the cathode.

As discussed in Section A-2, the back-bombardment energy is bounded by minimum and maximum values given by Equations (38) and (39), which are very close in value at low power but diverge appreciably at high power especially for near-cycloidal trajectories, $\rho \sim 1$. The minimum value does not depend on power level, but is realized only after the drift time T_s has passed. This value is plotted in Figure A-6. It is seen that this minimum bombardment energy is zero for a cycloid but is equal to V_o, the beam potential for $\rho = 0, 2$.

The maximum value is greater than the minimum value by a term which depends on power level and ρ (cf Equation 39), being proportional to ρ. The factor of proportionality to ρ is the back-bombardment energy of a cycloid. This has a maximum value at $\phi_o \sim \pi$ and is plotted as a function of power level in Figure A-7. This energy is only 10 - 20% of V_o for the low power range of 0.1 - 1 kw, which may be characteristic of the input section or buildup period of the typical CFA. At high power levels ~10 - 100 KW, which may characterize the output region in the steady state for this example, the bombardment energy is of the order of V_o. The result for 100 kW is not expected to be accurate because of the inception of nonadiabatic conditions in the electron trajectories.

The total maximum bombardment energy for any ρ and $\phi_o = \pi$, is plotted in Figure A-8 as a function of power level. This maximum value is slightly higher than the minimum by 10 - 20% in the range of 0.1 - 1 kW where the values of $(V_{bb}/V_o)_{max}$ are generally less than 0.5 except for the least likely trajectories of $\rho = 0.1$, $\rho = 1.9$. At high power levels, $(V_{bb}/V_o)_{max}$ is of the order of 1, except for the less likely trajectories $\rho = 1.9$, and $\rho = 1.5$.

Assuming random phases of orbital motion, one can expect the average value of (V_{bb}/V_o) for adiabatic trajectories to be the mean of the minimum and maximum values plotted in Figures A-6 and A-8. The mean value is greater than the minimum by about 0.1 - 0.2 at low power levels and by about 0.5 at high power levels. It is to be noted that the values in Figure A-8 are the maximum values expected for any ρ which will occur at $\phi_o = \pi$, for which the phase ϕ_s in the bombardment point is also roughly equal to π. For electrons at initial phases other than $\phi_o = \pi$, the values drop off by the factor $|\cos \phi_s|$ (the second term of Equation 39) so that for a large portion of the range ϕ_o, especially at ρ much different from unity, the bombardment energies approach the minimum value expected.

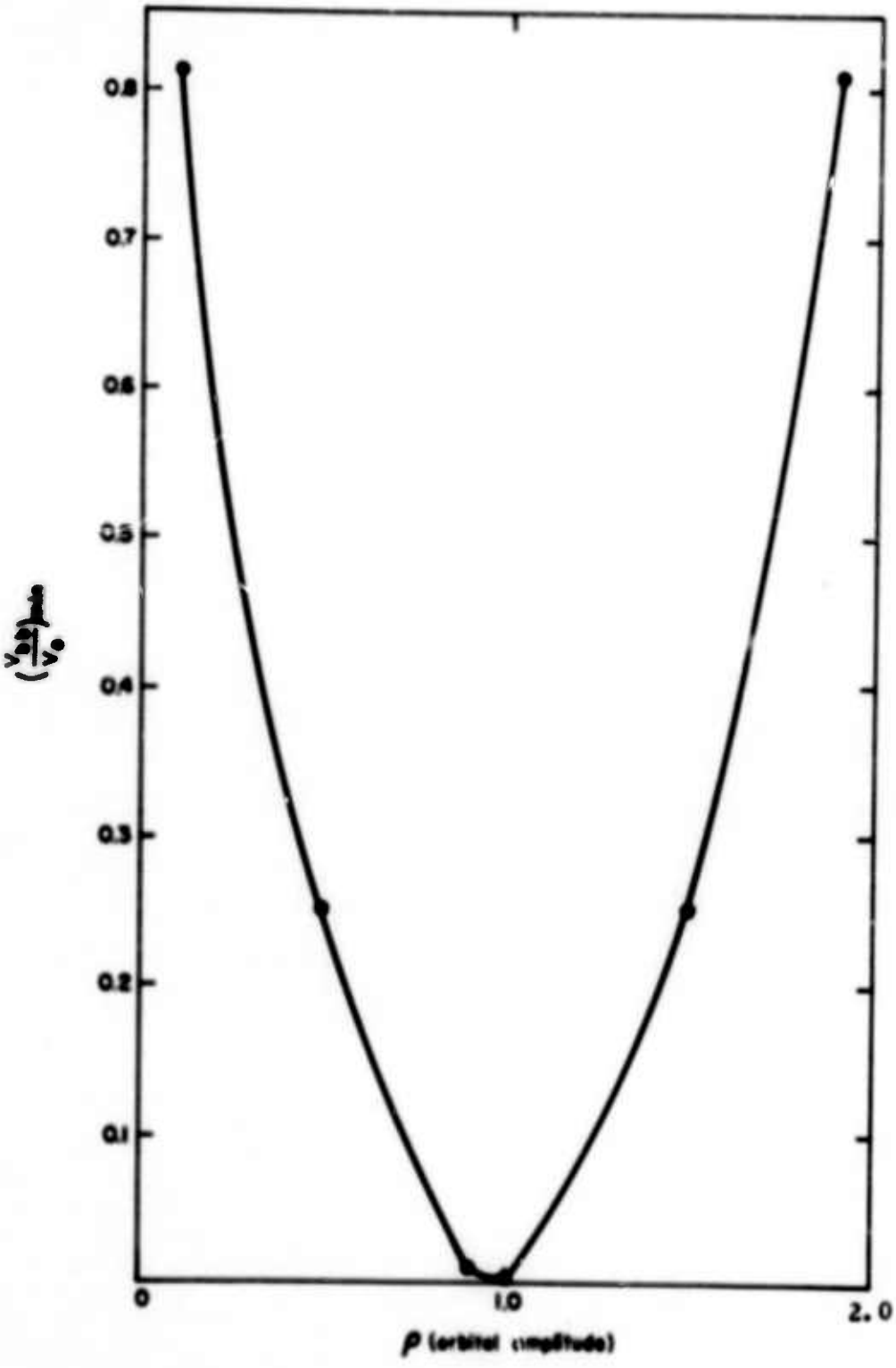

Figure A-6. Minimum Bombardment Energy Under Adiabatic Conditions as a Function of Orbital Amplitude

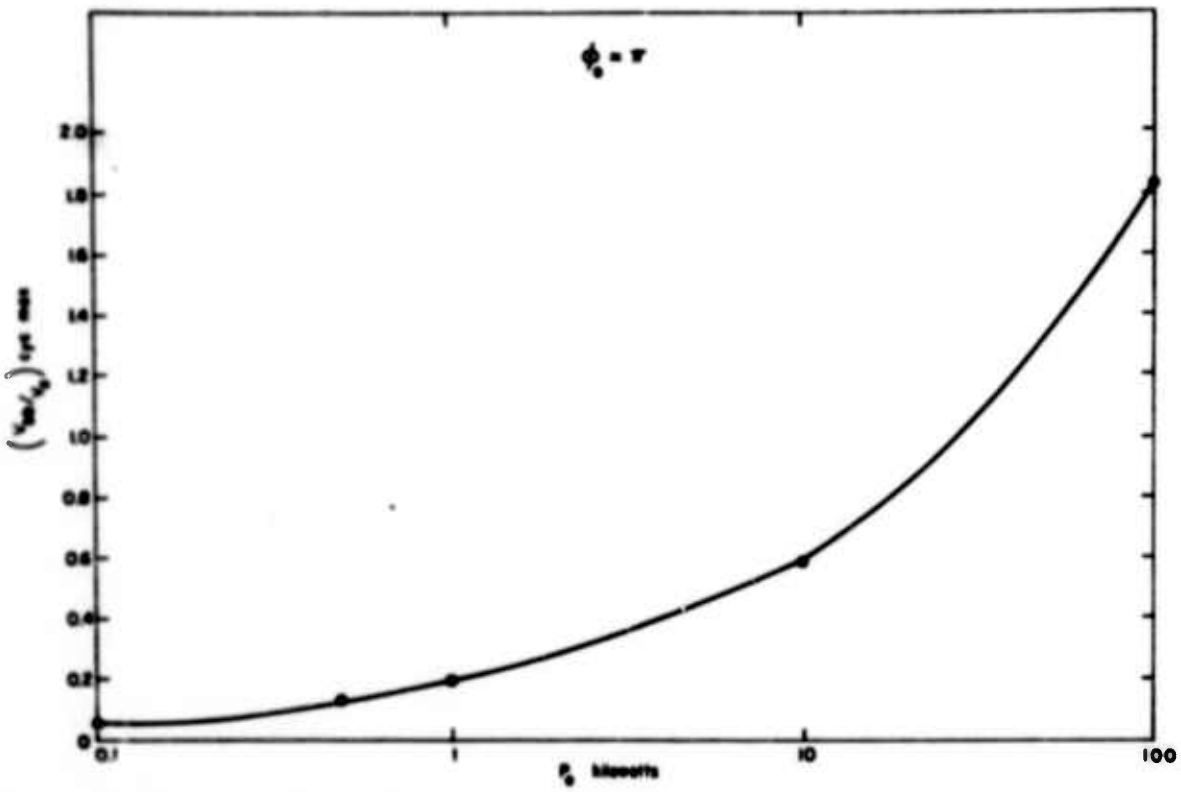

Figure A-7. The Maximum Bombardment Energy for a Cycloid as a Function of Power Level

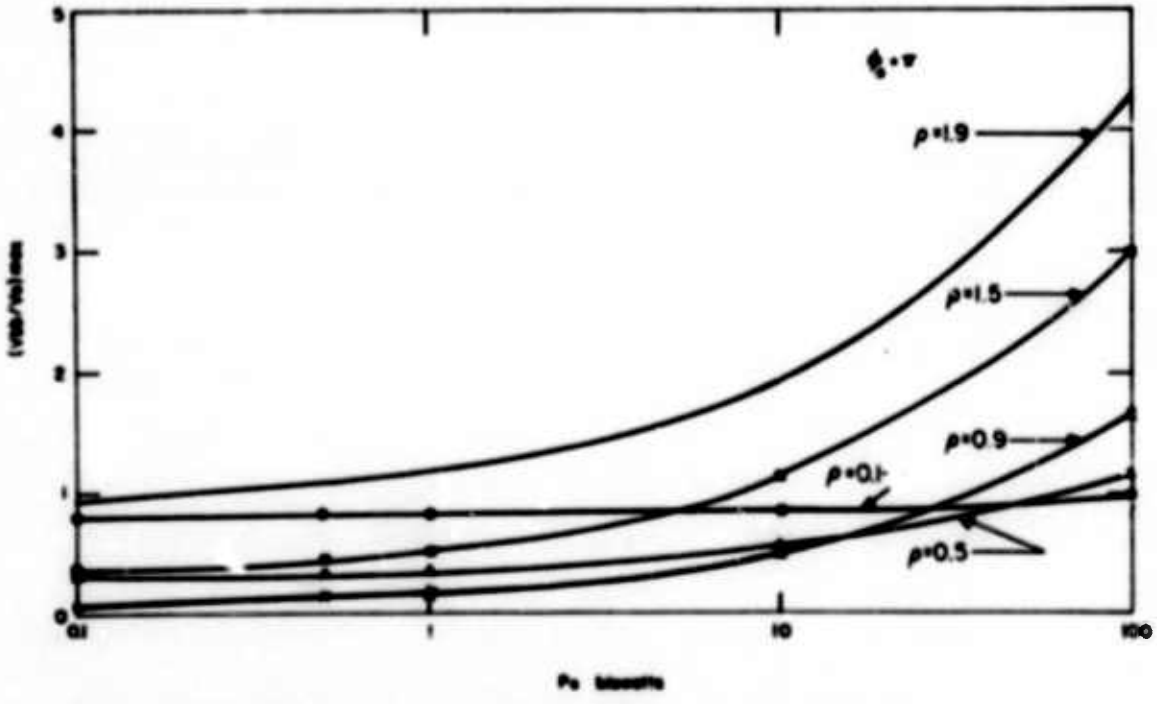

Figure A-8. Maximum Bombardment Energy under Adiabatic Conditions as a Function of Power Level and Orbital Amplitude

In general, one can conclude that, for the less likely trajectories with ρ quite different from unity, the back-bombardment properties, including bombardment energy, are close to the minimum and independent of power level except for the dependence of drift time on power. For near cycloidal trajectories, which are more likely, the bombardment properties are strongly dependent on power level.

It was pointed out in Section A-2 that adiabatic trajectories in general, except for ρ close to unity, will bombard the cathode at near-grazing incidence, i.e., $\theta_{in} \sim \pm \pi/2$ in Figure A-3. The greatest deviation from grazing will occur when $\phi_s \sim \pi$, according to Equations (43) and (44). The deviation increases as the quantity θ, $o < \theta < \theta_{max}$ increases from zero. The value of θ_{max} corresponds to the angle of incidence of a cycloid and its dependence on power level is shown in Figure A-9. Whereas the incidence of a cycloidal trajectory changes from normal toward grazing as power increases, the angle of incidence, for a trajectory of ρ quite different from unit, changes from grazing toward normal as power increases, albiet slowly in the case of $\rho = 0.1$. These features are illustrated in Figure A-10 for five values of ρ. In each case it should be remembered that the result represents the maximum deviation from grazing incidence. The average angle of incidence is closer to grazing than the value shown in Figure A-10. The distribution of angles of incidence is thus closely confined to near-grazing (90°) for $\gamma = 0.1$, hover around 70° for $\rho = 0.5$, increase from 30 to 45° for $\rho \sim 0.9$, and assume positive and negative values for $\rho = > 1$. The case $\rho = 1.5$ shows the angle of incidence varies from $\sim -60^\circ$ to $+30^\circ$ as power is increased, with normal incidence occurring at ~10 kW. Normal incidence for $\rho = 1.9$ occurs at 30 kW, showing that increasing ρ tends to yield a negative angle of incidence.

Estimates of the distribution and the average value of the principal back-bombardment properties were obtained for the assumed beam distribution $w = \sin \rho \pi/2$. Since only five values of γ were used, although equal increments of 0.1 were used for ϕ_s, the number of samples is limited and the resulting distributions are jagged but probably represent the expected smooth curve adequately for the present purposes.

The distributions of drift time were similar at all power levels. The one for 0.5 kW is shown in Figure A-11. There is a sharp peak at about T_s equal to one-half cyclotron period, corresponding to the predominance of cycloids for the trajectories of the bombarding electrons. The great majority of electrons intercept the cathode by the time of 6 cyclotron periods. The few values of T_s at around 30 cyclotron periods correspond to the few electrons of $\rho = 0.1$ which intercept the cathode. The abscissa scale varies with power level approximately as the square root corresponds to the dependence of τ on P_o. Actually the values of T_s are uncertain by one cyclotron period corresponding to the uncertainty of the phase of orbital motion at the instant of collection. Therefore, the peak is actually at roughly one cyclotron period.

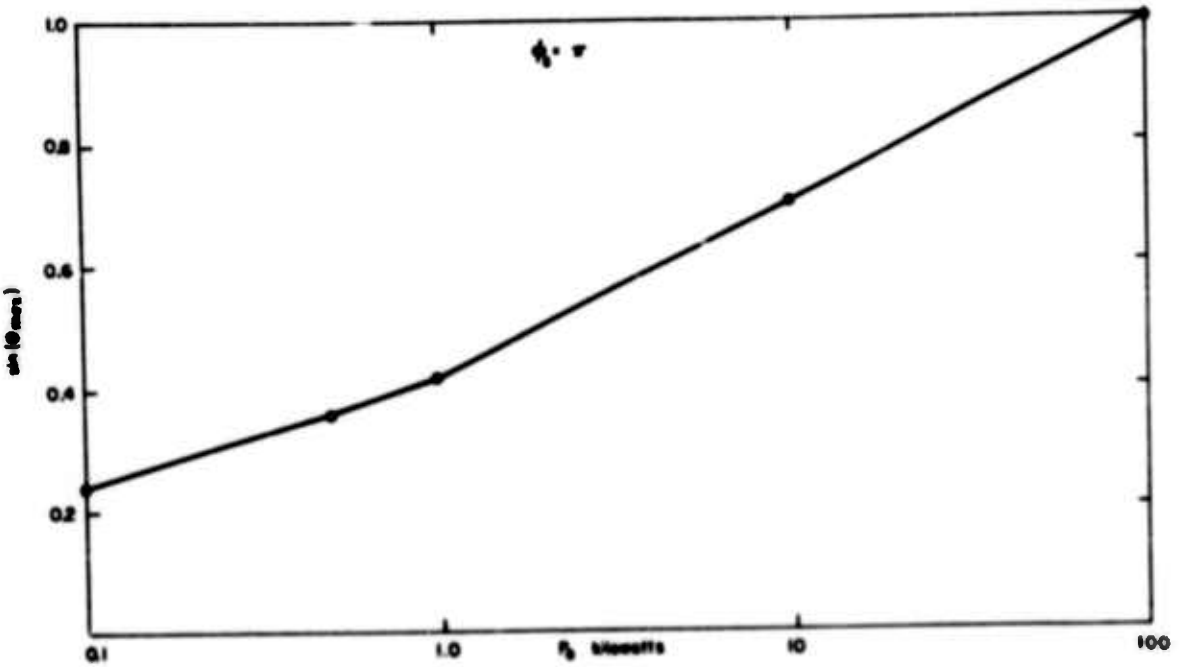

Figure A-9. Sine of the Angle of Bombardment (with Respect to Grazing Incidence) for a Cycloid in the Moving Reference Frame

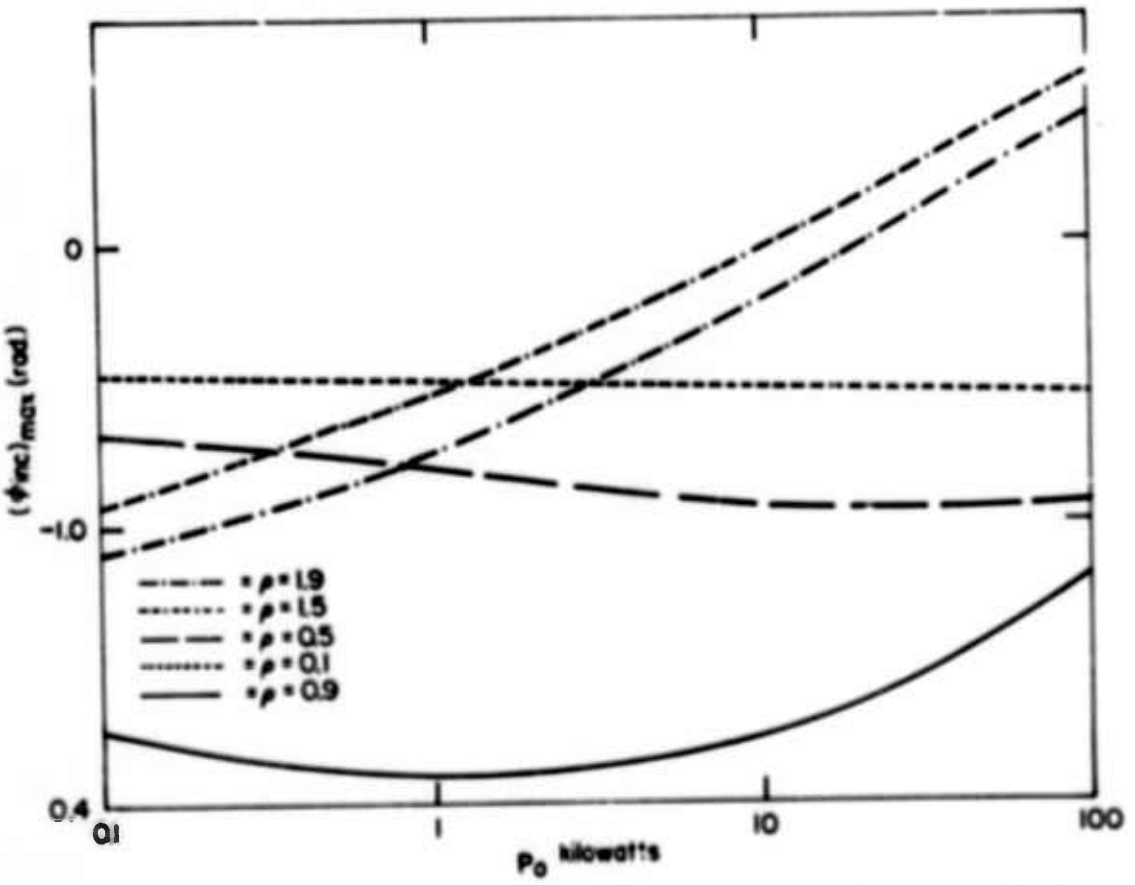

Figure A-10. The Maximum Angle of Incidence (with Respect to Normal Incidence) for Electrons of Various Orbital Amplitude as a Function of RF Power Level

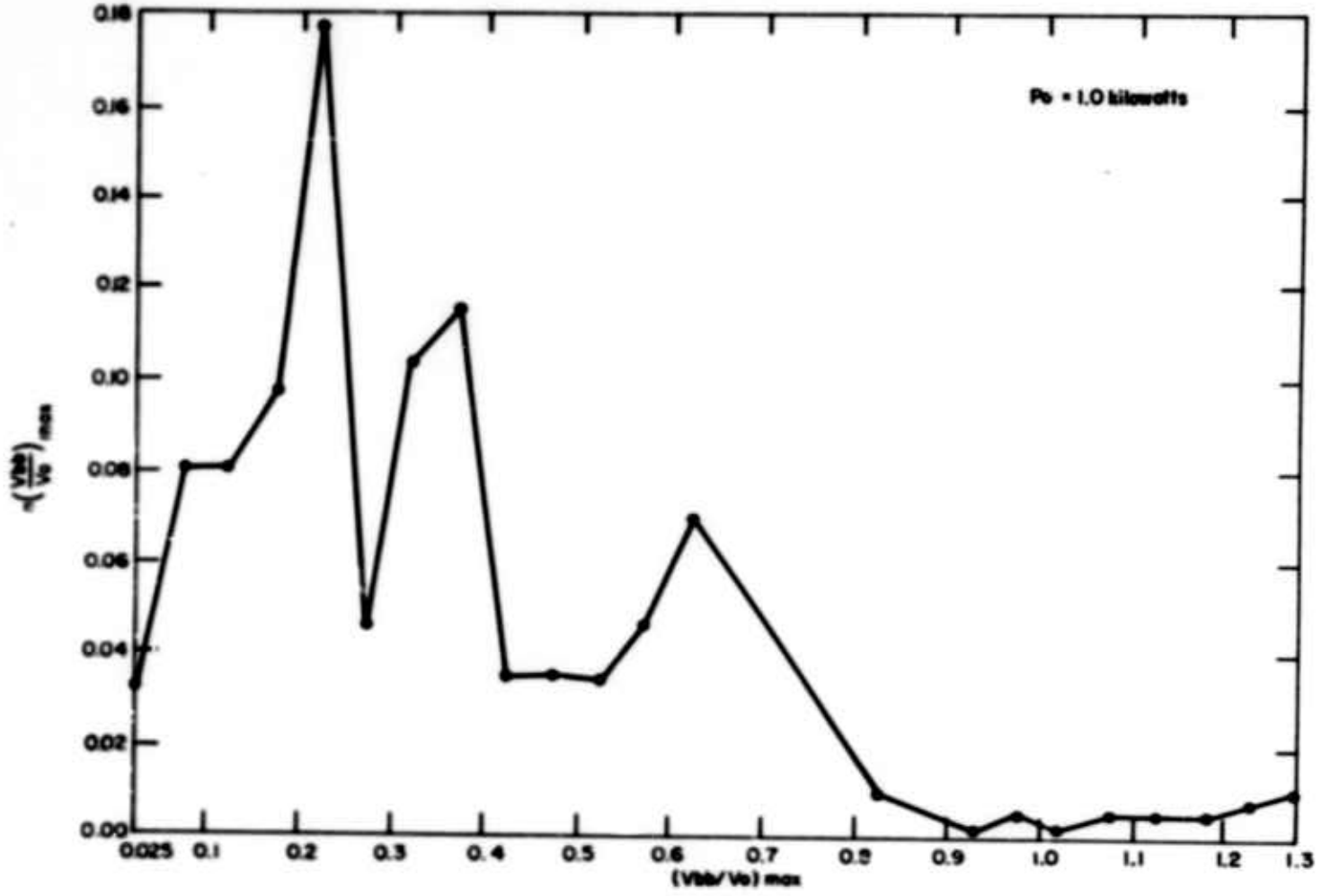

Figure A-11. Typical Distribution of Drift Time for Electrons in a Beam Composed of a Distribution of Orbital Amplitudes ρ given by $W(\rho) = \sin \rho \pi/2$

The average drift times for the electrons of the assumed beam which reach the cathode are illustrated in Table A-1.

Table A-1. Average Drift Time of Adiabatic Case

P_o (kilowatts)	T_s/T_c
0.1	5.5
0.5	2.9
1.0	2.1
10.0	1.1
100.0	0.6

The average value of the minimum bombardment energy for the assumed beam is about 0.17 V_o. This result again reflect the predominance of near-cycloidal electrons in those electrons which reach the cathode.

A typical distribution for the maximum bombardment energy is shown in Figure A-12. The disjointed curve is a result of the small number (5) of unequally distributed values of ρ used in the computation. The result is adequate to permit the observation again that near-cycloidal trajectories predominate since the principal peak (in this case at 0.22) is due to the near-cycloidal trajectory $\rho = 1$.

The average values of the bombardment energies for the assumed beam are tabulated in Table A-2.

Table A-2.

Bombardment Energies of Beam Under Adiabatic Motion

P_o (kw)	$(\overline{V_{bb}/V_o})_{min}$	$(\overline{V_{bb}/V_o})_{max}$	$(\overline{\frac{V_{bb}}{V_o}})_o$ - mean or most probable value
0.1	0.17	0.22	0.20
0.5	0.17	0.29	0.23
1.0	0.17	0.34	0.26
10.0	0.17	0.71	0.44
100.0	0.17	1.88	1.03

It is only for power levels less than 0.1 kW that the mean or most probable bombardment energy is that of the minimum associated with the adiabatic solution, without the correction for energy transfer on the last cyclotron period before collection. This observation is in parallel with the observation that the mean drift time (Table A-1) is as long as 10 or more cyclotron periods only at power levels below 0.1 kW.

At low power levels, 0.1 - 1 kW, the mean bombardment energy is about 0.25 V_o. This is probably applicable to an input region on the build-up phase. The high power level of 100 kW yields a predicted mean value of $\sim V_o$ for the bombardment energy, but this is presumably modified by the

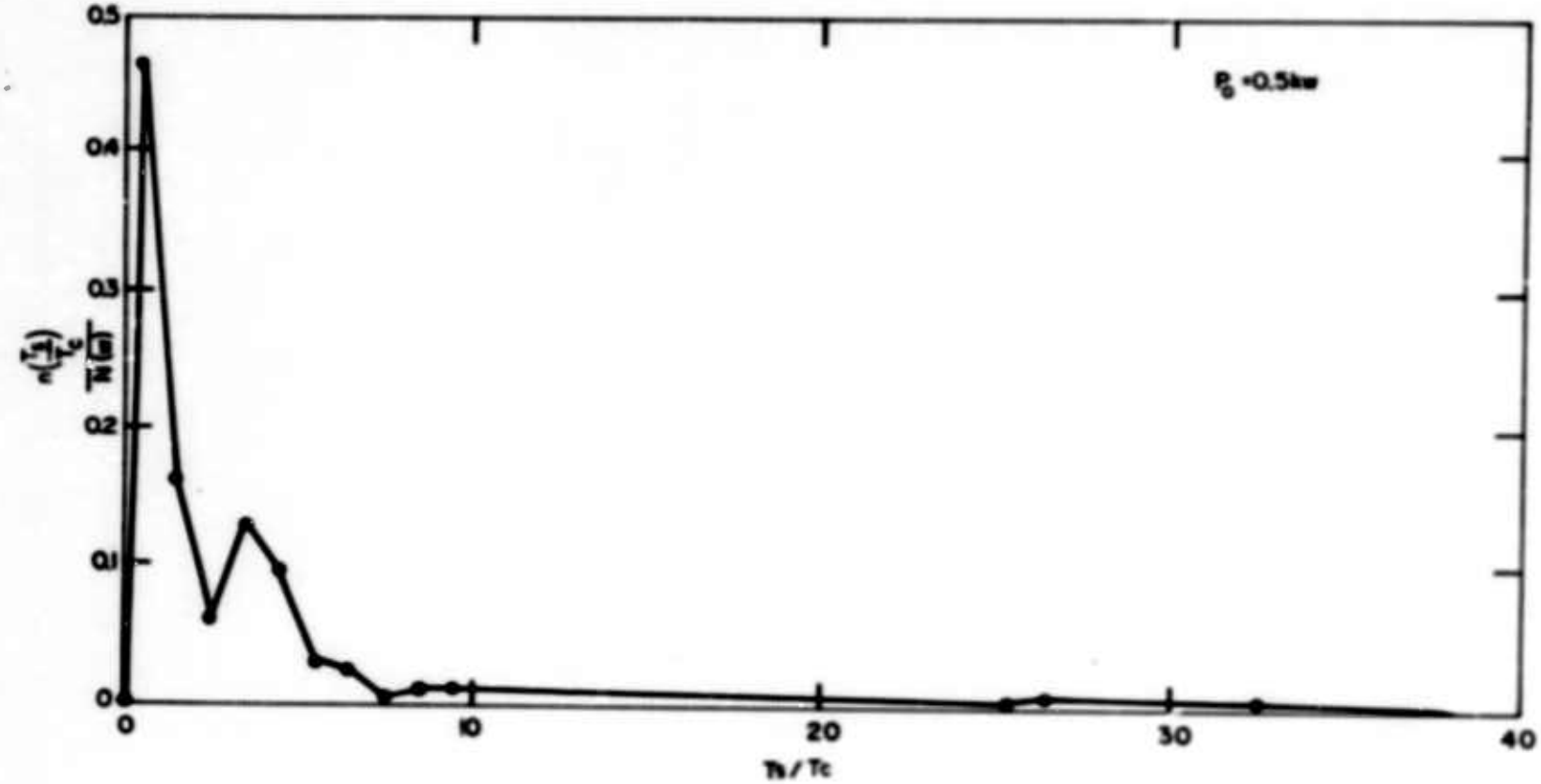

Figure A-12. Typical Distribution of Maximum Bombardment Energy in a Beam Composed of a Distribution of Orbital Amplitudes ρ Given by $W(\rho) = \sin \rho \pi/2$

onset of nonadiabatic conditions. There exists a minimum bombardment energy which persists as power level decreases. This is because the assumed beam contains trajectories other than cycloidal whose bombardment energies from adiabatic motion are independent of rf power and result theoretically after sufficient drift time. The cycloidal trajectory is unique in yielding a bombardment energy which decreases with power level with no limiting value – i. e., it decreases to zero as $\sqrt{P_o}$.

The electrons of the assumed beam exhibit a wide variety of angles of incidence at low power, from grazing to within 30° of normal incidence as shown in Figure A-13. The quantity plotted is the density of the maximum deviation from grazing incidence. Therefore, most electrons are closer to grazing than that class which has maximum deviation from grazing for a given ρ, the latter being the class described in Figure A-13. For this class, the predominance of cycloids is illustrated by the fact that higher power levels leads to a distribution (e.g., the one for 1.0 kW in Figure A-13) which is peaked toward the normal incidence value – i. e., about 30° from normal.

Table A-3 summarizes the mean value of the departure from grazing angle of incidence (90° or 1.57 radians) for the class of electrons exhibiting the maximum departure and the overall beam.

Table A-3.

Summary of Mean Values of Angle of Incidence for Adiabatic Beam Bombardment

P_o (kw)	$(\overline{\theta_{inc}})_{max}$ (radians)	$(\overline{\theta_{inc}})_{min}$ (radians)	$(\overline{\theta_{inc}})$ (radians)	(overall average, most probable values)
0.1	1.57 (grazing)	0.88	1.23	
0.5	1.57	0.75	1.17	
1.0	1.57	0.70	1.14	
1.5	1.57	0.56	1.07	
1.9	1.57	0.69	1.13	

It is clear that angles of incidence for the beam electrons vary from grazing to within 30° of the normal at all power levels, but the overall most probable value is about 60° from normal incidence and is not too sensitive with respect to power level. These are, of course, crude deliberations, since the distributions of (θ_{inc}) are examined with reference to the associated distribution of V_{bb}.

Despite the crudeness of the statistical analysis, it is reasonable to assume that the adiabatic beam is characterized in this typical CFA by: average drift times of several cyclotron periods, decreasing to one period at high powers; average bombardment energies of 0.20 V_o at low power (0.1 kW) and V_o at high power; and average angles of incidence of about 60° from normal, although the distribution of angles of incidence includes considerable near-grazing angles, especially at low power.

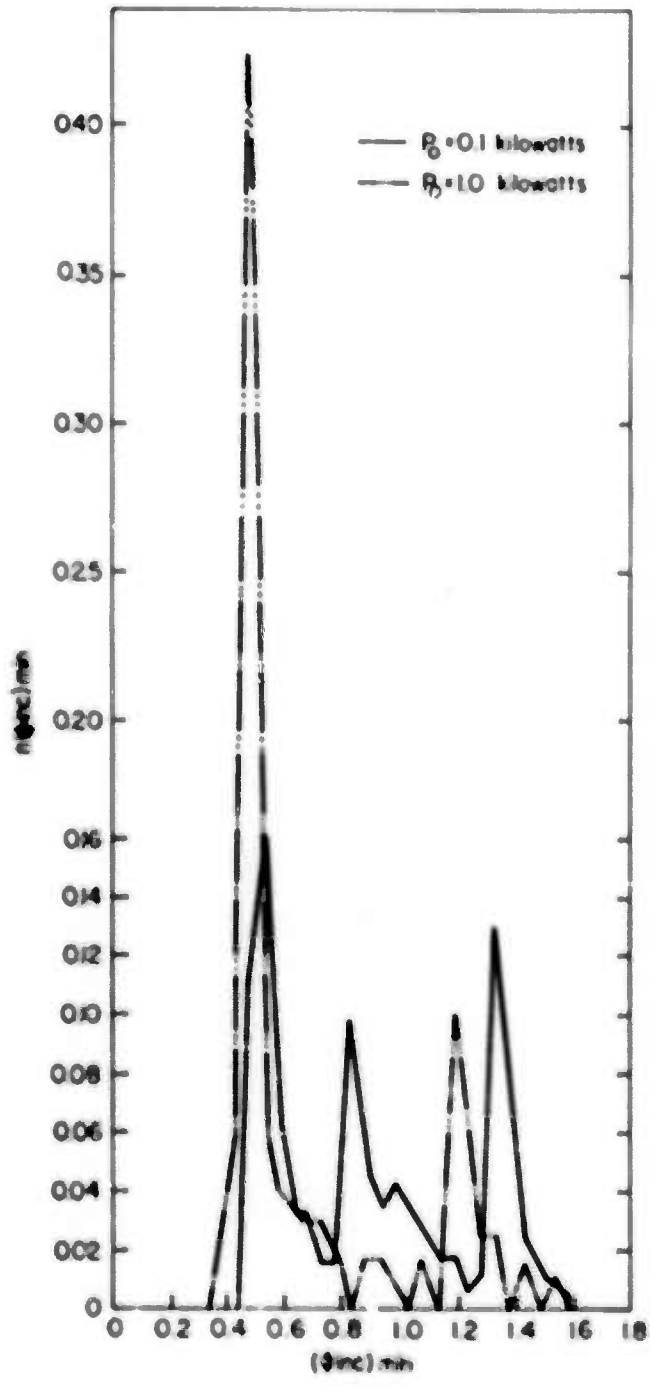

Figure A-13. **Typical Distribution of Angles of Incidence for a Beam Composed of Orbital Amplitudes p Given by W (p) = sin p π/2**

A-3.2 Cycloidal beam bombardment. A generalized beam as studied under the adiabatic case displays a greater variety of behavior depending on the trajectory than the cycloid; the latter appears to be unique in the process of CFA cathode back-bombardment and secondary emission. Thus, a separate review of the properties of a cycloidal beam bombardment is in order.

The bombardment energy depends simply on ϕ_o and τ/T_c as in Equation (49). The maximum value occurs at $\phi_o = \pi$ and is plotted in Figure A-7. The distribution of back-bombardment energy at a given power level is computed simply and is proportional to

$$d\phi / \frac{V_{bb}}{V_o} ;$$

viz.

$$n\left(\frac{V_{bb}}{V_o}\right) = \frac{2}{\pi} \frac{d\phi}{d\left(\frac{V_{bb}}{V_o}\right)_{cyc}} = \frac{\sqrt{\frac{1}{\pi}\left(\tau/T_c\right)}}{1 - \frac{\frac{V_{bb}}{V_o}\frac{\tau}{T_c}}{2}}^2 . \qquad (55)$$

This distribution is plotted for $P_o = 0.5$ kW in Figure A-14. It shows a sharp peak at the maximum value of ~ 0.125, corresponding to $\phi_o \sim \pi$, and an almost uniform density of $1/\pi\,(\tau/T_c)$ for the lower energies below 0.10. The average value of bombardment energy is

$$\left(\frac{V_{bb}}{V_o}\right)_{cgc} = \frac{(4/\pi)}{(\tau/T_c)} . \qquad (56)$$

For this example the average value is $\overline{V_{bb}} = 0.082\ V_o$.

The angle of incidence is given by Equations (50) and (51). The incidence is normal at low power and progresses towards grazing as power is increased. The dependence on bombardment energy is shown in Figure A-15. At a fixed power level, the electrons at $\phi_o \sim \pi$ would exhibit the greatest deviation from normal, whereas the electrons near $\phi_o \sim \pi/2$, $3\pi/2$, would exhibit near-normal incidence.

One other important quantity in the bombardment process is the phase shift of the secondary trajectory with respect to the primary. For cycloidal bombardment, this quantity is given by Equation (53) and is plotted vs ϕ_o for the five power levels in Figure A-16. We see that there is a particular phase ϕ for which the phase shift is zero. This value is close to $\pi/2$ for low power and progresses toward π as power is increased. The maximum phase shift is small at low power (e.g., +0.13 radians at 0.1 kW), insuring many steps of a multiplication sequence of secondaries, but at high power, e.g. 10 kW, where $\Delta\phi$ is large (up to 1.4 radians for 100 kW), secondaries escape from the bombardment region quickly and the multiplication sequence is quite limited.

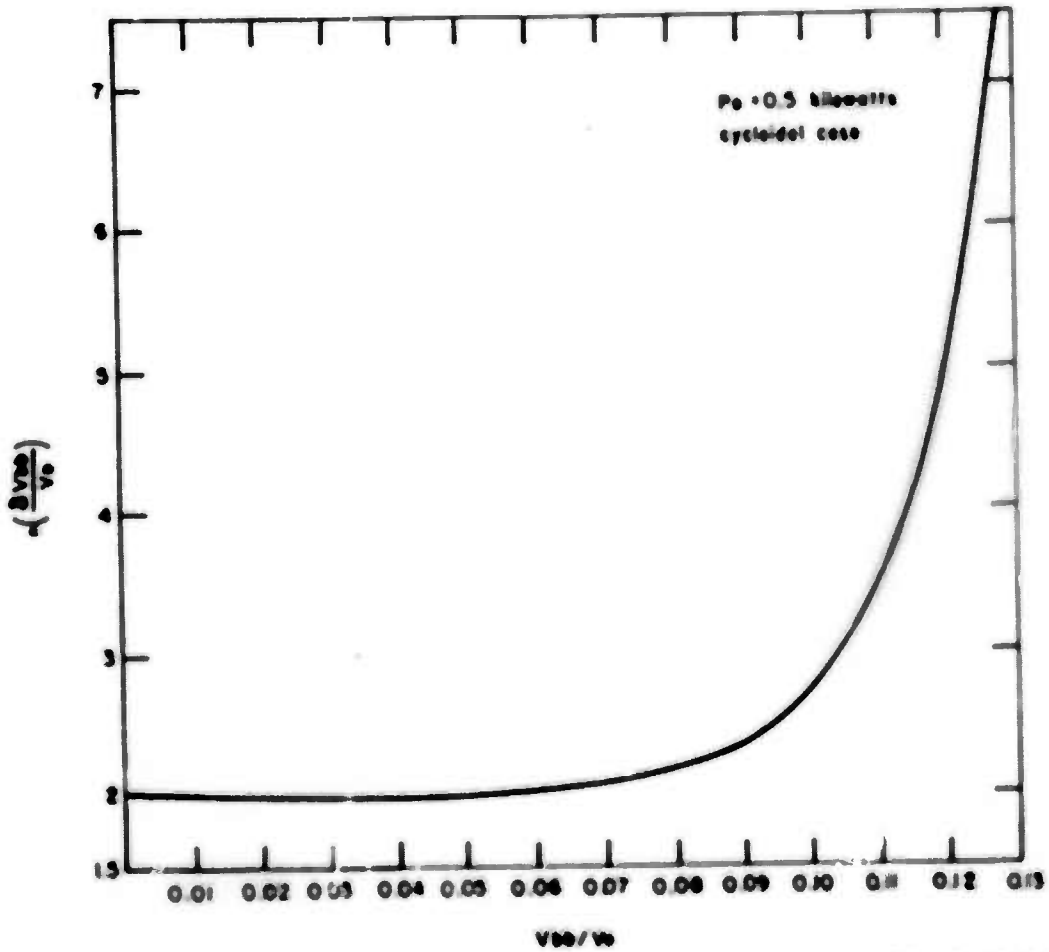

Figure A-14. Distribution of Bombardment Energy for a Cycloidal Beam

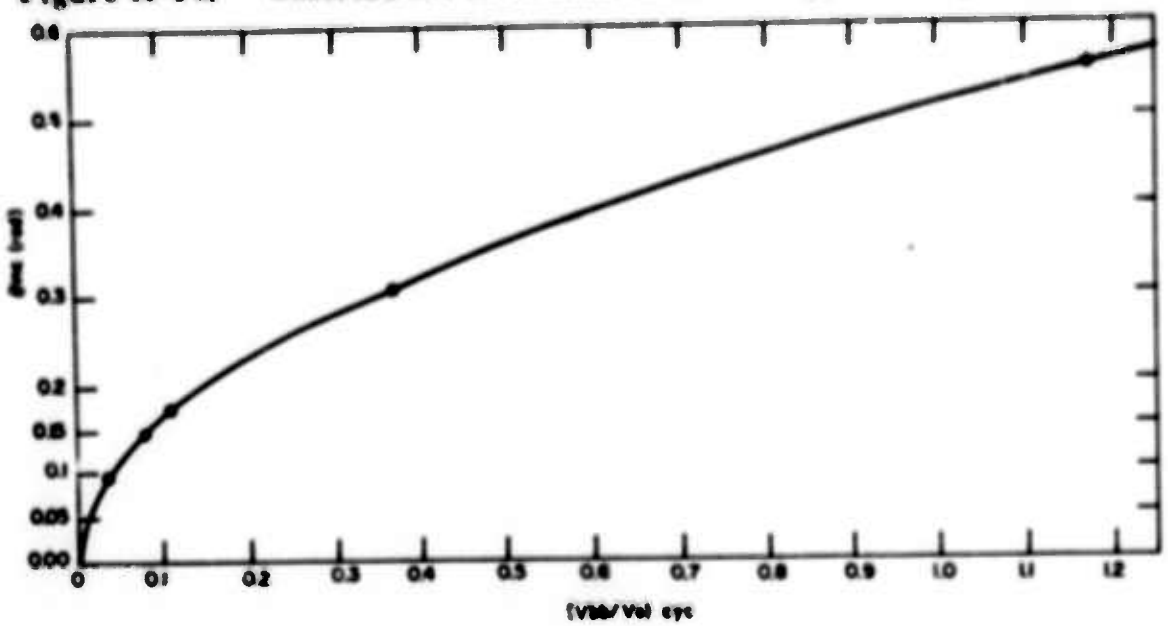

Figure A-15. Angle of Incidence as a Function of Bombardment Energy for a Cycloidal Trajectory

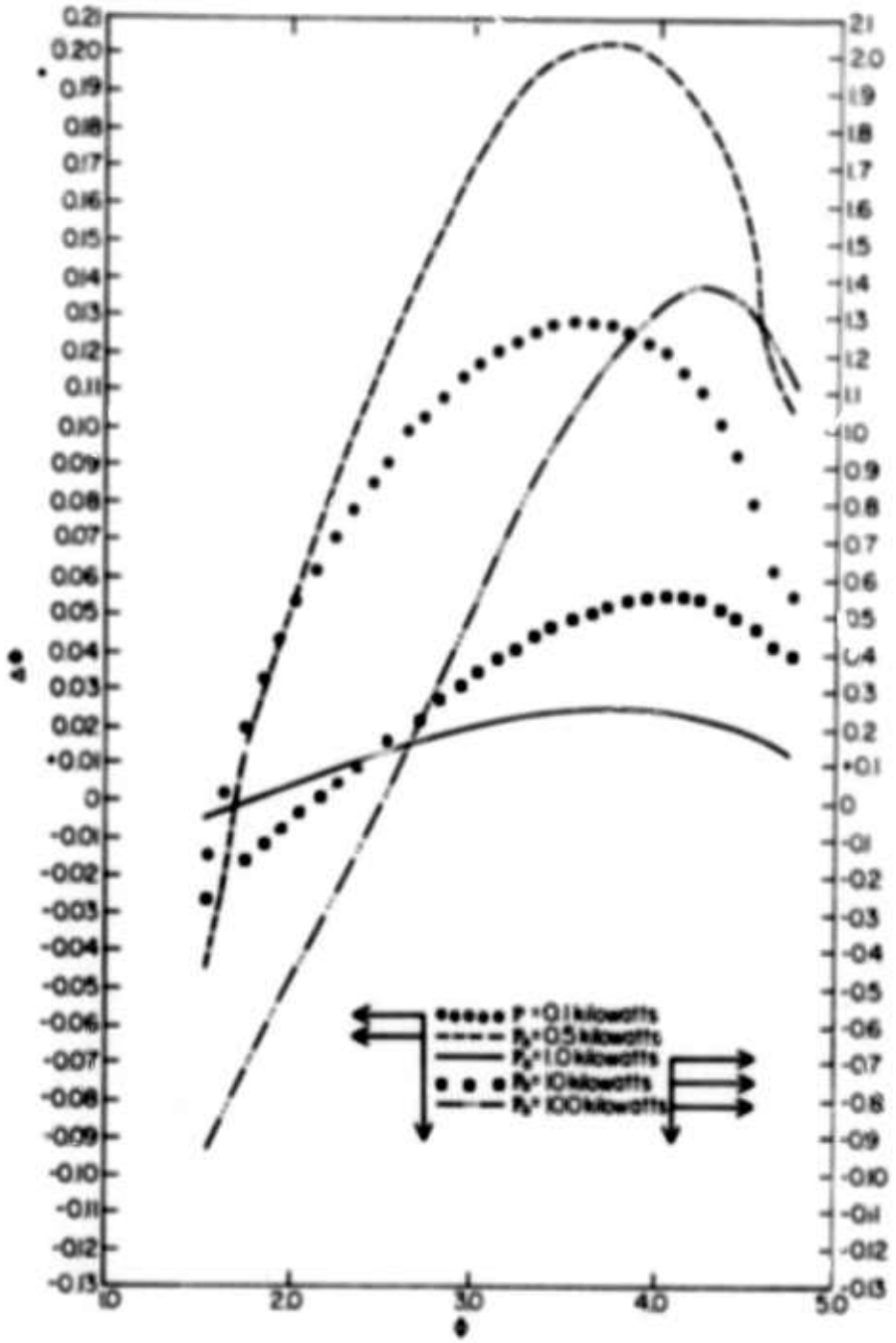

Figure A-16. The Phase Shift of a Secondary with Respect to a Primary in the Case of Cycloidal Bombardment as a Function of Initial Phase and Power Level

The principal features of the bombardment with cycloidal trajectories are summarized in Table A-4.

Table A-4.

Back-Bombardment Properties with Cycloidal Trajectories

P_o (kW)	$(\frac{V_{bb}}{V_o})_{o\ max}$	$(\frac{V_{bb}}{V_o})$	θ_{inc} at $\phi_o = \pi$ (radians)	θ_{inc} for V_{bb} (radians)	ϕ_e (radians)	$\Delta\phi_{max}$ (radians)	$\Delta\phi_{min}$ (radians)
0.1	0.056	0.036	0.11	0.10	1.63	+ 0.13	-0.015
0.5	0.125	0.082	0.18	0.15	1.73	+ 0.20	-0.05
1.0	0.177	0.115	0.21	0.17	1.78	+ 0.25	-0.08
10.0	0.56	0.364	0.37	0.30	2.11	+ 0.55	-0.28
100.0	1.77	1.15	0.70	0.55	2.50	+ 1.4	-0.92

The values of V_{bb} and θ_{inc} for $\phi_o = \phi_e$ are of particular interest because electrons near this phase initiate the longest sequences of secondary emission multiplication. These are listed in Table A-5 and compared with the values of θ_{inc} and V_{bb} at the point of maximum bombardment energy, $\phi_o = \pi$. Also listed is the phase shift $\Delta\phi$ at $\phi_o = \pi$, and the maximum number of multiplication sequences that can arise from an electron $\phi_o = \pi$.

Table A-5.

Comparison of Bombardment Properties at ϕ_e and $\phi_o = \pi$ (Assuming Velocity Synchronism)

	← $\phi_o = \pi$ →				← $\phi_o = \phi_e$ →		
P_o (kW)	$\frac{V_{bb}}{V_o}$	θ_{inc} (radians)	$\Delta\phi$ (radians)	N_{max}	$\frac{V_{bb}}{V_o}$	θ_{inc} (radians)	$\Delta\phi$ (radians)
0.1	0.056	0.11	0.12	~13	0.004	0.03	0
0.5	0.125	0.18	0.18	~ 9	0.02	0.06	0
1.0	0.177	0.21	0.21	~ 7	0.037	0.09	0
10.0	0.56	0.37	0.38	~ 4	0.29	0.27	0
100.0	1.77	0.70	0.63	~ 2	1.42	0.62	0

It would seem that V_{bb} is too small to yield a secondary emission ratio $\delta > 1$ for $\phi_o = \phi_e$ at low power, so that, at low power, the maximum secondary emission should originate from bombardment at $\phi_o \sim \pi$. However, since N_{max} decreases considerably with power, we might suspect that the limit on N would limit the emission. Actually, the best conditions for secondary emission multiplication in a tube of finite length probably exist with $\phi_o \sim \pi$ (± 20%) and the beam and circuit wave velocities unequal - i.e., off synchronism. This would introduce an additional phase shift and by this means $\Delta\phi$ could be adjusted to be zero at $\phi_o \sim \pi$. The required change in $\Delta\phi$ demands operation at voltages or beam velocity below synchronism. At beam velocities above the synchronism value, the existence of some ϕ_e in the range $\pi/2 < \phi_o < 3\pi/2$ soon disappears, which would denote the beginning of the loss of secondary emission multiplication.

At velocity synchronism, the value of ϕ_e is given by

$$|\sec \phi_e| - |\cos \phi_e| = \frac{\chi}{2\pi} \frac{\sinh \gamma_o d}{\left(\cosh \frac{\chi}{2} \gamma_o d\right)^2} \frac{V_a}{2R_c(d)P_o} . \qquad (57)$$

This shows $\phi_e \sim \pi/2$ at low power and $\phi_e \sim \pi$ at high power. There is a moderate amount of dependence of ϕ_e on $\gamma_o d$, χ, and V_a but it seems that the flexibility of adjusting ϕ_e by off-synchronism interation is the more significant factor in a reasonable picture of the multiplication process and the conditions required for its existence.

A-4. CONCLUSIONS

The back-bombardment properties of space-charge free electron trajectories in a CFA have been calculated. Two cases were distinguished: (1) beams composed of a variety of trajectories and (2) beams of only cycloidal trajectories. For most processes in the distributed emission cold cathode CFA, whether re-entrant or non-reentrant, the second case is more applicable, whether during a buildup phase or in a steady state. Only in the initial bombardment in the input region of a CFA would the first case be of interest, provided there was an input beam as results in the re-entrant CFA.

The first case, or general adiabatic beam case, is characterized by long drift times before bombardment (i.e., the order of 10 at low power); high values of back-bombardment energy $V_{bb} \sim 0.20\ V_b$ grazing to about 45° from the normal. Even in this case, the near-cycloidal trajectories tend to dominate the results because of their greater probability of capture by the cathode. Nevertheless, the presence of trajectories sufficiently far from cycloidal results principally in the possibility of a considerable V_{bb} value at low power, at the expense of longer drift time.

The second case, or cycloidal case, applies to the multiplication process, whether initiated by a cycloidal beam or general adiabatic beam. This case is characterized by a back-bombardment energy proportional to the beam potential V_o and the square root of the power level. Thus, at low power, the maximum V_{bb} is less than results in the adiabatic case (e.g., in the example studied, the cycloidal case yields a maximum V_{bb} of $0.056\ V_o$ at 0.1 kW as compared to $0.22\ V_o$ in the adiabatic case). A value of $V_{bb} \sim 0.20\ V_o$, however, is obtained in this example for the cycloidal case at a power level of 1 kW, which is roughly 20 db below the saturation power level. At 10 db below saturation power level, the bombardment energy is roughly about $0.4\ V_o$. The angles of incidence are close-to-normal in general, except at high power where the deviation from normal may be as much as 30° or more.

The important properties of cycloidal beam bombardment include the existence of an initial phase ϕ_e for which the phase shift of secondaries with respect to primaries is zero. This phase is adjustable within the range of $\pi/2 - 3\pi/2$ by off-synchronism interaction. It is thus speculated that the

initial buildup, and also the steady-state process, with low drive occurs with $\phi_e \sim \pi$, and below-synchronism interaction. In this way a continuing source of initiation of the multiplication process moves along with the wave.

Although the cycloidal process characterized by low V_{bb} and low θ_{inc} at low power is most significant for the cold cathode CFA, it is conceivable that higher V_{bb} and more grazing incidence of bombarding electrons could be achieved for low power by inducing non-cycloidal trajectories. This could be accomplished by appropriate corrugations or periodic sawtooths in the cathode surface. Such techniques have been said to be significant in yielding variation of cathode back-bombardment in magnetrons.

The back-bombardment energy V_{bb} varies as $|\cos \phi_o|$ in the range of unfavorable interaction phase $\pi/2 < \phi_o < 3\pi/2$. This simple result, indicating a maximum bombardment at $\phi_o = \pi$ or somewhat greater than π because of phase shift corresponds to results of Feinstein.[3]

Feinstein's results are for a planar magnetron and based on a model assuming a Brillouin space-charge hub which is not essentially disturbed in dc properties as the rf motion of initially synchronous electrons move from or through the space charge. This would seem unrealistic but it permitted Feinstein to obtain some numerical results in a simple manner. His power level value of f = 0.01, 0.1, correspond approximately to power levels of roughly 0.5 and 50 kW respectively in this study. Table A-6 compares his principal results for back-bombardment energy with those of this study.

Table A-6.

Comparison of Back-Bombardment Energy from Feinstein and this Study

← Feinstein Study →			← Present Study →			
Parameter f	$(\frac{V_{bb}}{V_o})_{o\ max}$	$(\frac{V_{bb}}{V_o})_{o\ min}$	P_o (kw)	$(\frac{V_{bb}}{V_o})_{o\ max}$ (cycloidal case)	$(\frac{V_{bb}}{V_o})_{o\ max}$ (adiabatic beam case)	$(\frac{V_{bb}}{V_o})_{o\ min}$
0.01	0.125	> 0	0.5	0.125	0.29	0.17
0.1	0.58	~ 0	50	1.25	1.31	0.17

The apparent agreement at f = 0.01 with the present results at 0.5 kW for the cycloidal case may be somewhat fortuitous since the distribution in Feinstein's results for this case is not as close to cosinusoidal as we expect for the cycloidal case. Since Feinstein's model implies essentially near-adiabatic motion from initially rectilinear trajectories, we have expected $V_{bb} \sim V_o$ in all cases or somewhat less. It appears, however, that in Feinstein's solution, the effect of space charge, in causing a variation of dc E field along the history of an electron drift is to cause the electron

to progressively assume a quasicycloidal trajectory. This trajectory will have a greater average dc velocity in the direction of the hub translation than the laminar velocity at the average position above the cathode.

For the high power level f = 0.1, Feinstein's results yield a value of V_{bb}, one-half of that in the present study. This can be explained by the greater rf electric field experienced by the cycloid of the present study at its maximum excursion toward the circuit, as compared to the lower rf fields experienced by the quasirectilinear trajectory in Feinstein's model.

In general, the magnitudes of V_{bb} agree, at least in order of magnitude, adequately enough for us to conclude that the cycloidal case results of the present study are reasonable, if we assume that near-cycloidal trajectories actually exist in cold cathode CFA's. This is certainly true during buildup and also is likely in the steady state.

Feinstein's results, it may be noted, have some peculiarities that cause some question of validity, especially at low power:

(1) The rf field distribution is assumed exponential, which is not correct at the cathode;

(2) the definition of slip in Equation (4) is not stated with complete consistency; and

(3) the results of his Figure A-7 show initially unfavorable electrons continuing to drift towards the cathode even after they have slipped into regions of favorable phase.

We may reasonably conclude that, for circuit-driven cold cathode devices, space-charge effects are secondary. In view of this, the Brillouin beam model is useful only as a gauge on current capacity of an interaction space. Certainly during the buildup phase, and probably in the steady state, space-charge effects are secondary. They should first appear in a modification of the assumed cyclotron frequency, and beam trajectory shape. The effective cyclotron frequency would be lowered and the cycloidal shape stretched out. In no case does the assumption of an initial laminar beam of full space-charge seem significant or of value for this problem.

With the neglect of space-charge, the optimum interaction for cold cathode secondary emission is close to that for optimum phase-focusing i.e., $\gamma_o d = 1.92$, compared to $\gamma_o d = 2.0$ for a given beam position and voltage. With $\gamma_o d \sim 1.5 - 2.0$, a reasonable choice of beam position for efficiency (e.g., $\chi \sim 0.5$) then results in an ω_c/ω value of 2.0.

It is interesting to compare these conditions with those for optimum cold cathode emission and interaction in the presence of a circuit, assuming that space-charge instability is a primary factor in the buildup process and bombardment process. Hartman[1] stages these conditions as $\omega_c/\omega = 2$, $\chi = 1/\pi$, and $\gamma_o d \sim \pi$.

If space-charge interaction is important, these latter conditions may be valid, but it is believed that circuit-driven cold cathode CFA's, especially in the initial buildup process, are quite independent of space-charge phenomena and are more likely to operate best under the conditions derived in this study.

A study of the probable multiplication sequences, utilizing the theory of cycloidal bombardment and the secondary emission characteristics of some known cathode material, would be of interest. It should be thus possible to deduce information on the threshold behavior and maximum power limits of cold cathode CFA's.

The maximum current boundary of a re-entrant cold cathode CFA is sometimes presumed to be due to the effective δ passing its maximum or even the upper crossover in the high power regions of the interaction space. It may be, however, that other effects, such as limitations on the multiplication sequence in cycloidal back-bombardment, could lead to a maximum current boundary before the effective δ of the material deteriorates.

It should be noted that if the cycloidal case of back-bombardment and secondary multiplication is valid in CFA's and magnetrons, then the assumption of interaction with only the velocity-synchronous spatial harmonic may be in error. Certainly in the magnetron, both forward-and backward-traveling fundamental harmonics must be taken into account because of the short interaction time of a cycloid. This leads to time modulation at the rf frequency of the secondary emission, which is likely to be quite important in the starting processes of the magnetron. In nonresonant CFA's, any spatial harmonic rf electric field of magnitude at the beam position comparable to the velocity-synchronous harmonic field must be taken into account. This could include backward-traveling harmonics as well as fast mode fields.

A-5. ACKNOWLEDGEMENT

The efforts of Miss Barbara Healy in compiling the numerical data are gratefully acknowledged.

This work was partially supported by the Raytheon Microwave and Power Tube Division, in connection with Contract No. DA 28-043-AMC-01698(E), "Long-Life Cold Cathode Studies for Crossed Field Tubes," L. Lesensky, Project Director.

REFERENCES

1. Hartman, C. W., "Production and Interaction of Electron Beams in Crossed Fields," University of California Report SR10, Electronics Research Laboratory (1961) (AD254709).

2. Collins, G. B., "Microwave Magnetrons," pp. 274-275, McGraw Hill, N. Y. (1948).

3. Feinstein, J., "Planar Magnetron Theory and Applications," Chap. 5-2-6 of Crossed-Field Microwave Devices 1, ed. E. Okress, Academic Press, N. Y. (1961).

Security Classification

DOCUMENT CONTROL DATA - R&D

(Security classification of title, body of abstract and indexing annotation must be entered when the overall report is classified)

1 ORIGINATING ACTIVITY (Corporate author)

Raytheon Company
Microwave and Power Tube Division
Waltham, Massachusetts

2a REPORT SECURITY CLASSIFICATION
UNCLASSIFIED

2b GROUP
N/A

3 REPORT TITLE

Long-Life Cold Cathode Studies for Crossed-Field Tubes

4 DESCRIPTIVE NOTES (Type of report and inclusive dates)

Fourth Quarterly Report - 15 July - 15 October 1966

5 AUTHOR(S) (Last name, first name, initial)

Lesensky L.; McGoech, C. R.

6. REPORT DATE	7a. TOTAL NO. OF PAGES	7b. NO. OF REFS
February 1967	62	3

8a. CONTRACT OR GRANT NO.	9a. ORIGINATOR'S REPORT NUMBER(S)
DA28-043-AMC-01698(E)	
b. PROJECT NO. 7900-21-223-12-00	PT-1286
c.	9b. OTHER REPORT NO(S) (Any other numbers that may be assigned this report)
d.	ECOM-01698-4

10. AVAILABILITY/LIMITATION NOTICES

This document is subject to special export controls and each transmittal to foreign governments or foreign nationals may be made only with prior approval of CG, USAECOM, ATTN: AMSEL-KL-TD, Fort Monmouth, N. J. 07703

11. SUPPLEMENTARY NOTES	12. SPONSORING MILITARY ACTIVITY
	U. S. Army Electronics Command Fort Monmouth, N. J. 07703 AMSEL-KL-TD

13. ABSTRACT

Secondary emission measurements of electron-beam-evaporated alumina films yielded δ_{max} values of approximately 5.0 with no apparent dependence on film thickness in the range 100 Å - 1000 Å.

Sputtering of 500 Å and 1000 Å electron-beam-evaporated alumina films with nitrogen indicated yields of 0.015 molecules/ion at 0.8 KV and 0.017 molecules/ion at 1.2 KV respectively.

The Hot-Cold Electron Bombardment Vehicle was completed and initial tests were performed. Targets requiring activation or high temperature processing will be evaluated.

The 50 kv S-band Amplitron test vehicle, QKS1194, was nearly completed during the present quarter.

Interest in and effort on the oxygen approach continues. A high average power version of the QKS1319 CFA test vehicle, which is under construction, will be used for life testing employing the oxygen approach.

An analysis of electron back-bombardment energy, angle of incidence, and phase shift in CFA's is given in the Appendix.

DD FORM 1473

Security Classification

Security Classification

14 KEY WORDS	LINK A		LINK B		LINK C	
	ROLE	WT	ROLE	WT	ROLE	WT
Electron-beam-evaporated alumina films Secondary emission measurements Sputtering Hot-Cold electron bombardment vehicle 50 kv, S-band Amplitron test vehicle, QKS11 94 Electron back-bombardment energy in CFA's						

INSTRUCTIONS

1. **ORIGINATING ACTIVITY:** Enter the name and address of the contractor, subcontractor, grantee, Department of Defense activity or other organization *(corporate author)* issuing the report.

2a. **REPORT SECURITY CLASSIFICATION:** Enter the overall security classification of the report. Indicate whether "Restricted Data" is included. Marking is to be in accordance with appropriate security regulations.

2b. **GROUP:** Automatic downgrading is specified in DoD Directive 5200.10 and Armed Forces Industrial Manual. Enter the group number. Also, when applicable, show that optional markings have been used for Group 3 and Group 4 as authorized.

3. **REPORT TITLE:** Enter the complete report title in all capital letters. Titles in all cases should be unclassified. If a meaningful title cannot be selected without classification, show title classification in all capitals in parenthesis immediately following the title.

4. **DESCRIPTIVE NOTES:** If appropriate, enter the type of report, e.g., interim, progress, summary, annual, or final. Give the inclusive dates when a specific reporting period is covered.

5. **AUTHOR(S):** Enter the name(s) of author(s) as shown on or in the report. Enter last name, first name, middle initial. If military, show rank and branch of service. The name of the principal author is an absolute minimum requirement.

6. **REPORT DATE:** Enter the date of the report as day, month, year; or month, year. If more than one date appears on the report, use date of publication.

7a. **TOTAL NUMBER OF PAGES:** The total page count should follow normal pagination procedures, i.e., enter the number of pages containing information.

7b. **NUMBER OF REFERENCES:** Enter the total number of references cited in the report.

8a. **CONTRACT OR GRANT NUMBER:** If appropriate, enter the applicable number of the contract or grant under which the report was written.

8b, 8c, & 8d. **PROJECT NUMBER:** Enter the appropriate military department identification, such as project number, subproject number, system numbers, task number, etc.

9a. **ORIGINATOR'S REPORT NUMBER(S):** Enter the official report number by which the document will be identified and controlled by the originating activity. This number must be unique to this report.

9b. **OTHER REPORT NUMBER(S):** If the report has been assigned any other report numbers *(either by the originator or by the sponsor)*, also enter this number(s).

10. **AVAILABILITY/LIMITATION NOTICES:** Enter any limitations on further dissemination of the report, other than those imposed by security classification, using standard statements such as:

(1) "Qualified requesters may obtain copies of this report from DDC."

(2) "Foreign announcement and dissemination of this report by DDC is not authorized."

(3) "U. S. Government agencies may obtain copies of this report directly from DDC. Other qualified DDC users shall request through

_____."

(4) "U. S. military agencies may obtain copies of this report directly from DDC. Other qualified users shall request through

_____."

(5) "All distribution of this report is controlled. Qualified DDC users shall request through

_____."

If the report has been furnished to the Office of Technical Services, Department of Commerce, for sale to the public, indicate this fact and enter the price, if known.

11. **SUPPLEMENTARY NOTES:** Use for additional explanatory notes.

12. **SPONSORING MILITARY ACTIVITY:** Enter the name of the departmental project office or laboratory sponsoring *(paying for)* the research and development. Include address.

13. **ABSTRACT:** Enter an abstract giving a brief and factual summary of the document indicative of the report, even though it may also appear elsewhere in the body of the technical report. If additional space is required, a continuation sheet shall be attached.

It is highly desirable that the abstract of classified reports be unclassified. Each paragraph of the abstract shall end with an indication of the military security classification of the information in the paragraph, represented as *(TS)*, *(S)*, *(C)*, or *(U)*.

There is no limitation on the length of the abstract. However, the suggested length is from 150 to 225 words.

14. **KEY WORDS:** Key words are technically meaningful terms or short phrases that characterize a report and may be used as index entries for cataloging the report. Key words must be selected so that no security classification is required. Identifiers, such as equipment model designation, trade name, military project code name, geographic location, may be used as key words but will be followed by an indication of technical context. The assignment of links, rules, and weights is optional.